



## Three-dimensional graphoepitaxial growth of oxide films by pulsed laser deposition

**Mozhaev, Peter B.; Mozhaeva, Julia E.; Khoryushin, Alexey V.; Hansen, Jørn Bindslev; Jacobsen, Claus S.; Bdikin, Igor K.; Kotelyanskii, Iosif M.; Luzanov, Valery A.**

*Published in:*  
Physical Review Materials

*Link to article, DOI:*  
[10.1103/PhysRevMaterials.2.103401](https://doi.org/10.1103/PhysRevMaterials.2.103401)

*Publication date:*  
2018

*Document Version*  
Peer reviewed version

[Link back to DTU Orbit](#)

*Citation (APA):*  
Mozhaev, P. B., Mozhaeva, J. E., Khoryushin, A. V., Hansen, J. B., Jacobsen, C. S., Bdikin, I. K., Kotelyanskii, I. M., & Luzanov, V. A. (2018). Three-dimensional graphoepitaxial growth of oxide films by pulsed laser deposition. *Physical Review Materials*, 2(10), Article 103401. <https://doi.org/10.1103/PhysRevMaterials.2.103401>

---

### General rights

Copyright and moral rights for the publications made accessible in the public portal are retained by the authors and/or other copyright owners and it is a condition of accessing publications that users recognise and abide by the legal requirements associated with these rights.

- Users may download and print one copy of any publication from the public portal for the purpose of private study or research.
- You may not further distribute the material or use it for any profit-making activity or commercial gain
- You may freely distribute the URL identifying the publication in the public portal

If you believe that this document breaches copyright please contact us providing details, and we will remove access to the work immediately and investigate your claim.

**Three-dimensional graphoepitaxial growth of oxide films by pulsed laser deposition**

Peter B. Mozhaev\* and Julia E. Mozhaeva

*Institute of Physics and Technology of the Russian Academy of Sciences, Moscow, 117218, Russia*

Alexey V. Khoryushin, Jørn Bindslev Hansen, and Claus S. Jacobsen

*Department of Physics, Technical University of Denmark, Kongens Lyngby, DK-2800, Denmark*

Igor K. Bdikin

*TEMA-NRD, Mechanical Engineering Department and Aveiro Institute of Nanotechnology (AIN), University of Aveiro, Aveiro, 3810-193, Portugal*

Iosif M. Kotelyanskii and Valery A. Luzanov

*Kotelnikov Institute of Radioengineering and Electronics of Russian Academy of Sciences, Moscow, 125009, Russia*

(Received 3 August 2018; published xxxxxx)

Metaloxide thin films were deposited on tilted-axes NdGaO<sub>3</sub> substrates (TAS NGO) by pulsed laser deposition. A specific growth mode resulting in an inclination between crystallographic planes of the top layer and that of the bottom layer was commonly observed. A simple geometrical growth model, taking into account faceting of the surface of the bottom layer, explains the observed dependencies well. The matching of the top and the bottom layer is essentially three dimensional, with graphoepitaxial matching in the substrate plane. The three-dimensional graphoepitaxial (3DGE) growth mechanism seems to be quite common for deposition on TAS with tilt angles more than 5°. It was observed for eight of ten studied combinations of materials, including multilayer heterostructures, for four different deposition techniques, and on substrates with different predeposition treatment. The 3DGE growth was observed both with increase and decrease of the top layer tilt angle compared to the tilt angle of the bottom layer. Two different 3DGE dependencies can be distinguished in the high-angle range (>15°): with a tendency towards standard growth above some threshold angle, and retaining 3DGE behavior until a tilt angle of 45° is reached, either by the top or by the bottom layer. In a simplified way the difference may be attributed to two different formation mechanisms: the first one generates the additional tilt when the growing grain overgrows another grain, seeded on the next step on the substrate surface, while for the second mechanism the inclination is formed when the grain is seeded over the step. The first type is better described by a tangent angular dependence, it is observed usually when a compressive strain is induced in the top layer. The second type follows a sine dependence, and is usually seen for a tensile-strained top layer.

DOI: [10.1103/PhysRevMaterials.00.003400](https://doi.org/10.1103/PhysRevMaterials.00.003400)**I. INTRODUCTION**

Deposition of epitaxial thin oxide films on substrates with inclination of surface orientation from the small-index crystallographic planes (SICPs)—the tilted-axes substrates (TAS), often also called “miscut” or “vicinal” substrates—is attracting more and more attention in the last decades as a simple way of preparation of quantum wires and quantum dots (see, e.g., [1]). Previously studies of oxide films deposition on TAS was usually pursuing the goal of improvement of the lattice perfection and surface smoothness due to change of the growth mechanism from 3D (Vollmer-Weber or Stransky-Krastanov modes) to the two-dimensional (2D) step-flow growth (see, for example, [2–4]). The reason for such a change is the surface structure of the TAS, representing a network of steps with terrace and edge surfaces oriented along the SICPs (see, e.g., [5]). The SICPs forming the terraces for some substrate materials and orientations are

called “habit planes,” because the standard deposition on these materials is done with substrate surface orientation along the “habit” SICP. This network of steps provides excellent seeding positions in the internal corners formed by the step edge and the surface of the next terrace, and force the unidirectional growth from the edge of the terrace [Fig. 1(a)]. The overgrowth of the grain seeded on the next joint of terrace and edge determines the general properties of the growing film: strain, orientation, dislocations density, and surface roughness. Note that the strain in the overgrowth area is generated not only by the in-plane mismatch due to the difference of the lattice constants of the film and the substrate, but also by the out-of-plane mismatch [not shown in Fig. 1(a)]. This “standard” growth mode [Fig. 1(a)] demonstrates good parallelism of crystallographic planes of the film and the substrate, and the strain, generated by the film-substrate lattice mismatch, is accommodated by generation of dislocations and step bunching (see, e.g., modeling in [6]). Some authors even claim this standard growth mechanism with parallel SICPs of the film and the substrate to be the only possibility.

\*Corresponding author: pbmozh@gmail.com

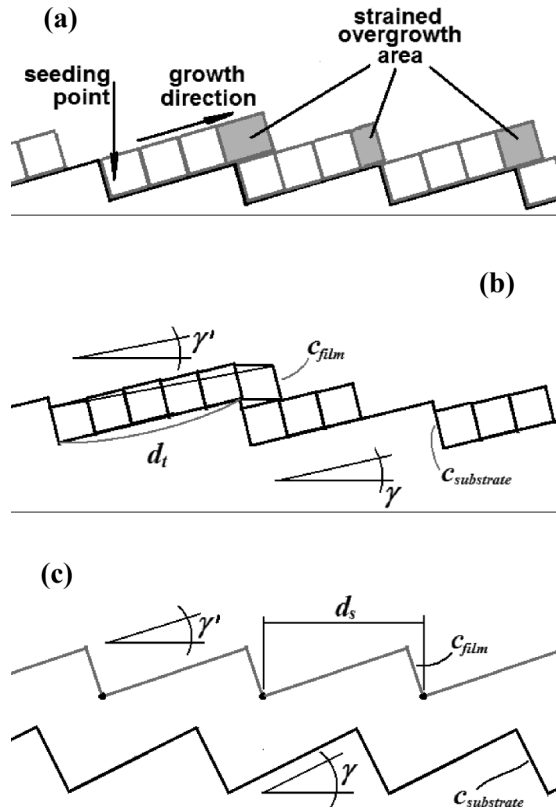


FIG. 1. Growth modes during oxide deposition on tilted-axes substrates: (a) Standard growth mode with parallel small-index crystallographic planes (SICPs) of film and substrate. (b) and (c) Three-dimensional graphoepitaxial growth mode with mutual inclination of film and substrate planes. (b) Overgrowth mechanism, when inclination between the SICPs of the substrate and the film is caused by a difference between the height of the substrate step and the layer thickness of the film on the next terrace. The case of smaller height of the growth step of the film is shown. The resulting tilt follows the tangent formula [Eq. (1) in text]. (c) Simultaneous seeding of the film on neighboring seeding knots (black dots) results in the sine model [Eq. (2)].

plane rocking curve of the film compared to the corresponding rocking curve of the substrate. The inclination mainly depends on the mismatch between the substrate and film, and for deposition on a substrate aligned along a SICP (habit plane) the crystallites are inclined randomly, or almost randomly, in the substrate plane. Systematic small-angle (usually below  $1^\circ$ ) tilt of the films SICP along some crystallographic direction in the substrate plane also manifests this second relaxation mechanism (see, e.g., [14]). The third epitaxial mode is a result of accommodation of strain by disconnections generated on the edges of the steps. The inclination of the film lattice depends on both lattice mismatch and substrate plane tilt from the habit plane and may be described in a simple geometric way first proposed by Nagai [8]. The height of the growth steps of the film  $c_f$  [Fig. 1(b)] is not equal to the height of the steps on the substrate surface  $c_s$ . As a consequence, the inclination of the crystallographic planes of the film from the substrate surface plane  $\gamma'$  increases compared to the substrate tilt  $\gamma$  when  $c_f > c_s$ , and decreases when  $c_f < c_s$ . Considering overgrowth of the layers (see, e.g., [15]) with average length of the terrace surfaces  $d_t$  [Fig. 1(b)], we can write the obvious relations

$$d_t = c_f / \tan \gamma' = c_s / \tan \gamma, \quad \gamma' = \arctan[(c_f / c_s) \tan \gamma]. \quad (1)$$

This simple formula may change if seeding is considered not in a single edge-terrace joint, but simultaneously on neighboring seeding knots (black dots in Fig. 1(c), [16]). In this case simple considerations provide the sine dependence instead of tangent:

$$d_s = c_f / \sin \gamma' = c_s / \sin \gamma, \quad \gamma' = \arcsin[(c_f / c_s) \sin \gamma], \quad (2)$$

where  $d_s$  is the average distance between the seeding knots on the substrate surface. Usually the authors do not distinguish the two possible mechanisms and use sine or tangent for their convenience, or even ignore the trigonometric functions and calculate the angle directly. The reason is the *vicinal* range of the tilt angles, in most of the studies less than  $5^\circ$  and only in some studies increasing to  $\sim 10^\circ$ .

It is important to note that  $c_f$  and  $c_s$  are not the lattice constants, but the heights of the steps of film and substrate, only in some cases being equal to the lattice constants of the materials in respective directions (normal to the corresponding habit plane). For example, the height of step can be  $1/2$  or  $1/3$  of the lattice constant ([17] and [15], correspondingly), or a fractional part of the translation distance in the cases when faceting happens along (110) or (111) SICPs.

This epitaxial growth mode is essentially three dimensional: the tilt axis of the substrate provides initial bonding conditions for the film, usually similar to the epitaxial relations on the habit plane, while the translation distance ( $d_t$  or  $d_s$ ) and the ratio of substrate to film step heights determines the mutual orientation of the habit plane of the substrate and the corresponding SICP of the film. The film and the substrate are coupled, thus, in all three dimensions, while for ordinary epitaxial growth the coupling occurs only in the substrate plane, i.e., in two dimensions. At the same time, this growth mechanism may be considered as a kind of graphoepitaxy,

In fact, studies of deposition of semiconducting thin films on TAS showed the possibility of different film-substrate orientational relations, depending on the mechanism of lattice-mismatch strain accommodation. The first observations of inclination of the SICPs of the film from that of the substrate date back to the early 1970s [7–10]. The mechanisms resulting in such inclinations were discussed in different ways in [11–13]. According to [13], three epitaxial modes are possible, with lattice mismatch accommodation by (i) dislocations with Burgers vector in the habit plane, (ii) dislocations with Burgers vector inclined relative to the habit plane, and (iii) disconnections generated on the edges of the terraces on the TAS surface. The first mode corresponds to the standard mode [Fig. 1(a)], with no inclination of the SICPs of the film from that of the substrate, and with the lattice-mismatch generated strain being completely relaxed by generation of dislocations. The second mode results in some (usually small) inclination of the lattice of the crystallites of the growing film, it is usually detected as an increased width of the out-of-substrate

141 because the orientation and structure of the film is determined  
 142 not exclusively by ions in the lattices of film and substrate,  
 143 but also by a net of features on the substrate surface with the  
 144 size greater than the interatomic distances or lattice constants.  
 145 To indicate all these features we will refer to this growth  
 146 mechanism as the three-dimensional graphoeptitaxial (3DGE)  
 147 growth mode.

148 The three mechanisms of mismatch relaxation may co-  
 149 incide, with corresponding change of inclination angle and  
 150 strain to some intermediate values between the pure cases  
 151 [13].

152 The 3DGE mechanism, fairly described with geometrical  
 153 approximation, was observed in numerous studies of semi-  
 154 conductor heteroepitaxy, references can be found in [11–  
 155 13]. Most of these heterostructures were limited to small tilt  
 156 angles (vicinal range), utilized in semiconductor technology  
 157 for improvement of thin film quality. Oxide thin films and  
 158 substrates were rarely studied and most of the obtained tilts  
 159 in oxide heterostructures were misinterpreted or left without  
 160 explanation.

161 To our knowledge, 3DGE in all-oxide heterostructures was  
 162 first observed in 1991 by Kotelyanskii and Luzanov [18],  
 163 when CeO<sub>2</sub> films were deposited on NdGaO<sub>3</sub> (NGO) TAS  
 164 (tilt around the [001] axis from the (110) plane towards  
 165 (010) plane) with e-beam evaporation. All range from (110)  
 166 to (−1 1 0) planes [orthorhombic notation, equivalent to the  
 167 (100)<sub>c</sub> and (010)<sub>c</sub> planes of the pseudocubic notation for  
 168 the NGO crystal] was studied. The ⟨110⟩ axis of the CeO<sub>2</sub>  
 169 film was bound to the [001] tilt axis of the substrate for all  
 170 TAS orientations. The inclination of the CeO<sub>2</sub> (001) SICP  
 171 from the sample surface monotonously increased surpassing  
 172 the increase of the substrate tilt angle, until (110) CeO<sub>2</sub>  
 173 orientation was reached at  $\gamma_c \approx 32^\circ$  [Fig. 2(a), solid line].  
 174 The faster increase of film tilt  $\gamma'$  compared to the substrate  
 175 tilt  $\gamma$  was due to greater lattice constant of the film (5.4  
 176 and 3.86 Å, correspondingly), and showed good agreement  
 177 with the simple formula (2). The film remained (110)  
 178 oriented with a wide spread of grains orientation (rocking curve  
 179 width  $\sim 5^\circ$ ) until  $\sim 58^\circ$  substrate tilt, when 3DGE started to  
 180 follow the (−1 1 0) crystallographic plane of the substrate,  
 181 symmetrically equivalent to the initial (110) NGO plane.  
 182 The reason for (110)-oriented film growth is the presence of  
 183 two symmetrically equivalent {110} SICPs on the substrate  
 184 surface, each of them showing no preference over the other  
 185 neither in the resulting tilt of the film, nor in the area of the  
 186 corresponding facets on the substrate surface. The critical tilt  
 187 angle at which the growth mode changes from 3DGE to (110)  
 188 oriented is given by simple formula [sine dependence of tilt  
 189 (2)]

$$\gamma_c = \arcsin[(c_s/c_f) \sin(45^\circ)]. \quad (3)$$

190  
 191 For CeO<sub>2</sub> deposition on NGO  $\gamma_c \approx 30.4^\circ$ , in a reasonable  
 192 agreement with the observed value.

193 The study of CeO<sub>2</sub>/NGO heterostructures was continued  
 194 using rf sputtering [19,20] and pulsed laser deposition (PLD)  
 195 techniques [16,21]. Much higher deposition rate during rf  
 196 sputtering (5–7 nm/min instead of 0.5 nm/min for e-beam  
 197 evaporation) resulted in a more complicated behavior [19,20].  
 198 Both standard growth mode (type I in [19,20]) and 3DGE

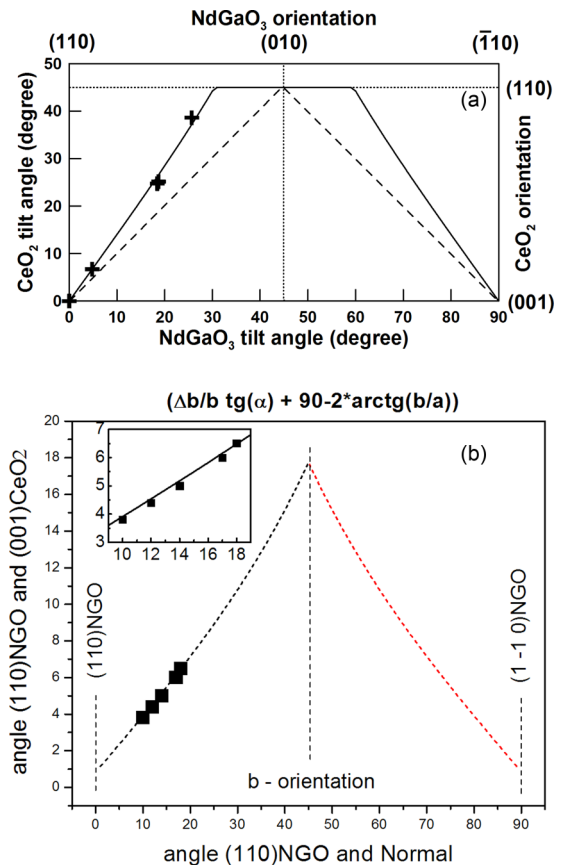


FIG. 2. First observations of gradual increase in tilt of crystallographic planes of the film in CeO<sub>2</sub> deposition on NdGaO<sub>3</sub> tilted-axes substrates. (a) With e-beam evaporation (solid line, [18]) and rf sputtering (crosses, [19,20]). The tilt of CeO<sub>2</sub> film with standard epitaxial growth mode is shown by a dashed line. (b) With PLD [22]. The formula on the graph takes into account the orthorhombicity of NdGaO<sub>3</sub>. Note that dependencies follow the sine formula [Eq. (1)] for (a) and the tangent formula [Eq. (2)] for (b).

199 growth mode (type II) are degenerated twice due to the pres-  
 200 ence of symmetrically equivalent (110) and (−1 1 0) planes  
 201 on the substrate surface. The angular dependence of the 3DGE  
 202 part of the film followed the same sine mode (2) as for  
 203 e-beam evaporation [Fig. 2(a), crosses]. Further increase of  
 204 the deposition rate for PLD (7–55 nm/min average deposition  
 205 rate, depending on the laser repetition rate, and above 100  
 206 nm/min peak deposition rate during the laser pulse) provided  
 207 3DGE growth in the 4°–20° substrate tilt angle range [21]. At  
 208 higher angles the inclination between the NGO (110) plane  
 209 and the CeO<sub>2</sub> (001) plane dropped to 2°–3° and remained at  
 210 this level over the range (23° <  $\gamma$  < 30°). Formula (1) was  
 211 applied to the 3DGE growth during PLD in [16] [Fig. 2(b)]  
 212 and showed excellent agreement with the observed mutual  
 213 film and substrate orientation. The more complicated view  
 214 of the formula in Fig. 2(b) compared to formula (1) is due  
 215 to an attempt to take into account the orthorhombic structure  
 216 of the substrate; in fact, this correction is small and may be  
 217 neglected. Deposition of YBa<sub>2</sub>Cu<sub>3</sub>O<sub>x</sub> (YBCO) over the CeO<sub>2</sub>  
 218 layer on NGO TAS resulted in a similar linear increase of the



219 film inclination and abrupt drop to  $\sim 2.5^\circ$  when  $\gamma$  exceeded  
220  $25^\circ$  [21].

221 PLD of  $\text{CeO}_2$  buffer layer on Ni biaxially textured tape  
222 with grain orientations randomly spread from the substrate  
223 surface plane was studied in [17]. At high deposition tem-  
224 peratures the out-of-substrate plane tilt of the (001) plane  
225 of the  $\text{CeO}_2$  overlayer follows the tilt of the (001) plane of  
226 the Ni grain below, but is smaller, in a qualitative agreement  
227 with the geometric formula. At low deposition temperature  
228 the crystallites of  $\text{CeO}_2$  are smaller than the terrace width  
229 on the Ni grain surface; this excludes the graphoepitaxial  
230 effect of steps on the film orientation, and, in fact, the  $\text{CeO}_2$   
231 film grows in an agreement with the standard growth mode,  
232 (001) $\text{CeO}_2$ ||((001)Ni) [17]. Authors mention that grains of  
233  $\text{LaMnO}_3$  and Y-stabilized  $\text{ZrO}_2$  (YSZ) also tilted according  
234 to the geometrical model when deposited on Ni tapes [17].

235 Similarly, in [15] another fluorite material, YSZ, deposited  
236 on the vicinal sapphire substrate [ $5^\circ$  from (0001) plane] with  
237 liquid phase epitaxy (LPE), showed mixed orientation from  
238 the standard growth mode to the 3DGE growth mode. The  
239 reason was intense step bunching on the substrate surface dur-  
240 ing substrate preparation (annealing at  $1500^\circ\text{C}$ ), resulting in  
241 broad (0001)-oriented terraces. Some of the YSZ crystallites  
242 were small enough to fit one terrace, and showed orientation  
243 (001)YSZ||((0001) $\text{Al}_2\text{O}_3$ ), while orientation of the big YSZ  
244 grains showed a tilt of  $5.9^\circ$ , in an excellent agreement with  
245 the geometrical model [15].

246 YBCO deposition by PLD on YSZ TAS and  $\text{CeO}_2$ -buffered  
247 sapphire TAS was demonstrated in [22]. Both cases showed  
248 3DGE, assuming that the  $\text{CeO}_2$  buffer layer is well oriented  
249 along the sapphire SICP: (001) $\text{CeO}_2$ ||( $1 - 1 0 2$ ) $\text{Al}_2\text{O}_3$ .  
250 We will discuss the results of [22] in more detail in the  
251 Discussion section below.

252 YBCO deposition on YSZ TAS was also studied in [23].  
253 Direct deposition resulted in  $c$ -oriented YBCO films inde-  
254 pendent of the substrate tilt angle, but introduction of a  
255 buffer  $\text{Y}_2\text{O}_3$  layer between YBCO and YSZ blocked chemical  
256 interaction and promoted film growth with a tilt of SICP. The  
257 inclination of the YBCO film from the habit plane shows the  
258 3DGE behavior (increase of the inclination with an increase  
259 of the substrate tilt angle), but the measured value of the film  
260 tilt is less than calculated using the simple formula (1). At  
261 high substrate tilt angle ( $35.7^\circ$ ) the YBCO film grows in the  
262 standard epitaxial mode with small (less than  $1^\circ$ ) deviation  
263 from the habit plane (001) YSZ [23].

264  $\text{PbTiO}_3$  deposition on  $\text{SrTiO}_3$  TAS [24] showed good  
265 agreement with the geometrical model, even though the mech-  
266 anism of growth is much more complicated than in other dis-  
267 cussed studies ( $a$ -oriented grains formation on the edges of the  
268 steps, with corresponding strains and distortions introduced  
269 into the  $c$ -oriented grains on the terraces). Another study of  
270  $\text{PbTiO}_3$  deposition on TAS, with  $\text{MgO}$  substrates [25], also  
271 resulted in the growth similar to the 3DGE, but with higher  
272 inclination of the film compared to the calculated using the  
273 table data.

274 Summarizing, the 3DGE growth mode is not something  
275 unusual for all-oxide heterostructures on TAS, but the mech-  
276 anism was quite often not recognized, and the results were  
277 misinterpreted. Systematic investigations of the growth mode  
278 are lacking, the angular ranges of 3DGE growth were not

279 determined. Deviations from the simple geometrical formula  
280 were not explained. At the same time, understanding of the  
281 3DGE mechanism is important for the fabrication of thin  
282 film heterostructures, especially when the materials are highly  
283 anisotropic, like high-temperature superconductors (HTSC)  
284 or piezoelectrics.

285 In this paper we present our observations of the 3DGE  
286 growth in different film-substrate pairs. Preservation of the  
287 3DGE growth mode through a multilayer system is demon-  
288 strated, and the characteristic features of the growth mode and  
289 deviations from the simple geometrical model are discussed.  
290 In this study we will concentrate on orientational characteris-  
291 tics of the 3DGE films and multilayers, the fabrication detail  
292 and secondary growth features will be presented in another  
293 publication.

## 294 II. EXPERIMENTAL TECHNIQUES

295 The TAS ( $5 \times 5 \times 0.5 \text{ mm}^3$ ) were cut from  $\text{NdGaO}_3$  sin-  
296 gle crystals, their substrate surface was set by tilting from  
297 the (110) habit plane around the [001] axis towards the  
298 (010) plane (corresponding to tilt around the [001] $_c$  axis  
299 from the (100) $_c$  plane towards the ( $-1 1 0$ ) $_c$  plane in the  
300 pseudocubic notation). The nominal tilt angle varied in the  
301 range  $0^\circ$ – $34^\circ$ . Chemical-mechanical polishing (CMP) of the  
302 substrates provided atomically flat surfaces with a roughness  
303  $R_a$  determined by atomic force microscopy (AFM) below  
304  $2 \text{ \AA}$ . Such a low roughness implies presence of a damaged  
305 “amorphous” layer on the surface of the substrate after CMP.  
306 Formation of pronounced steps on the surface with terraces  
307 and edges oriented along the {110} planes (surface recrystal-  
308 lization) demanded additional treatment: wet etching with HF  
309 and high-temperature annealing in oxygen (to be published).  
310 Mainly depositions were done on the as-polished substrates,  
311 only after rigorous cleaning in organic solvents and weak acid  
312 to remove contaminants present after dicing and CMP. The  
313 actual tilt orientation and angle of the substrate surface were  
314 checked after CMP with XRD measurements. The deviation  
315 of the actual tilt axis from the [001] axis of  $\text{NdGaO}_3$  did not  
316 exceed  $5^\circ$ , being usually less than  $2^\circ$ . The actual tilt angle was  
317 measured for each substrate.

318 Fluorite YSZ and  $\text{CeO}_2$ , perovskite  $\text{BaZrO}_3$  (BZO), and  
319 perovskitelike YBCO thin films were deposited in differ-  
320 ent combinations with PLD. The details of the technique  
321 can be found in [26]. Commercially available stoichiometric  
322 high-density ( $>90\%$  of bulk density) ceramic targets were  
323 used. The structural properties of thin films and multilayers  
324 were studied using x-ray diffraction techniques, the surface  
325 morphology was observed by SEM and AFM. Electrical  
326 properties of the superconducting films were measured with  
327 noncontact techniques. The complete results of our studies,  
328 including morphology and electrical properties of the films,  
329 will be published elsewhere: in this article we will concentrate  
330 only on the orientational features of the heterostructures.

331 The chosen film and substrate materials provided a wide  
332 range of lattice mismatch and corresponding strain introduced  
333 into the upper layer. The translation distances at room tem-  
334 perature and expected strain in the habit plane (110) NGO  
335 are presented in Table I for all studied top layer/bottom layer  
336 combinations. The lattice mismatches, in fact, differ from the

TABLE I. Lattice parameters of the substrate and film materials.

Top layer	Translation distances <sup>b</sup> (Å)		Calculated in-plane strain <sup>a</sup> (%)			
			Y : ZrO <sub>2</sub>	CeO <sub>2</sub>	BaZrO <sub>3</sub>	YBa <sub>2</sub> Cu <sub>3</sub> O <sub>x</sub>
Bottom layer	in-plane	out-of-plane				
NdGaO <sub>3</sub> Orthorhombic	3.861 × 3.864 <sup>c</sup>	3.861	+5.7– + 5.8	+1.0– + 1.1	–8.7– – 8.8	–0.75– + 1.0
Y : ZrO <sub>2</sub> Cubic	3.641 <sup>d</sup>	5.149	xxx	–5.0	–15.4	–6.8– – 5.1
CeO <sub>2</sub> Cubic	3.822 <sup>d</sup>	5.405		xxx		–1.8– – 0.1
BaZrO <sub>3</sub> Cubic	4.20	4.20			xxx	+7.4– + 8.9
YBa <sub>2</sub> Cu <sub>3</sub> O <sub>x</sub> Orthorhombic	3.825 × 3.89	3.89–3.92 <sup>e</sup>				xxx

<sup>a</sup>Negative value corresponds to compressive strain, positive to tensile strain.

<sup>b</sup>“In-plane” data are provided for the standard (110) orientation of the NGO substrate and corresponding SICPs of the films. Lattice structure and parameters are given for room temperature.

<sup>c</sup>Orthorhombic lattice of NdGaO<sub>3</sub> results in orthogonal translation directions on the (110) plane with distances  $c/2 = 3.864$  Å and  $[(a^2 + b^2)^{1/2}]/2 = 3.861$  Å.

<sup>d</sup>Fluorite lattice during deposition on perovskite NdGaO<sub>3</sub> substrate is tilted in substrate plane by 45° and the in-plane translation distances corresponding to the substrate axes are calculated as  $5.149/2^{1/2} = 3.641$  and  $5.405/2^{1/2} = 3.822$  Å for YSZ and CeO<sub>2</sub>, respectively.

<sup>e</sup>Perovskitelike lattice of YBCO consists of three perovskite cells in  $c$  direction, so the out-of-plane translation distance is given by  $c/3 = 3.89$ – $3.92$  Å, depending on the oxygen contents in the film.

337 presented, as a result of different thermal expansion coeffi-  
 338 cients, but since the lattices of both layers can be distorted by  
 339 the substrate-induced strain, by presence of oxygen vacancies,  
 340 and by chemical interaction between layers, we cannot present  
 341 exact values of the strain and keep the room-temperature data  
 342 as a reference. Actual strain should be determined for each  
 343 top layer/bottom layer combination using the measured lattice  
 344 constants in the fabricated heterostructures.

345 The deposition parameters for CeO<sub>2</sub> and YSZ were op-  
 346 timized to obtain smooth thin films of single orientation  
 347 (001)CeO<sub>2</sub>|(110)NGO on a standard (110)NGO substrate.  
 348 Substrate temperature during deposition was held at 740 °C,  
 349 the target was ablated at an energy density of 1.1 J/cm<sup>2</sup> and  
 350 pulse repetition rate of 2 Hz in a mixture of argon and oxygen  
 351 (6% O<sub>2</sub>, 0.2 mbar total pressure). Low energy density just  
 352 above the ablation threshold (~1 J/cm<sup>2</sup> in our deposition  
 353 system) resulted in a very low growth rate (~0.3 Å/pulse =  
 354 0.6 Å/s for CeO<sub>2</sub> and ~0.1 Å/pulse = 0.2 Å/s for YSZ),

and low oxygen partial pressure promoted growth of a film  
 of high crystal quality. No post-deposition annealing was  
 performed; the film was cooled down to room tempera-  
 ture in the working atmosphere at the maximal possible  
 rate.

The lattice constant of the YSZ films on (110) NGO  
 substrates was typically 5.145–5.155 Å, for some samples  
 ranging from 5.135 to 5.185 Å, in good agreement with  
 standard value of 5.15 Å. The FWHM (full width at half  
 maxima) of the peaks on the  $\theta/2\theta$  scans for the YSZ films  
 was very close to the estimations of the size broadening,  
 implying high homogeneity and low strain in the films. The  
 CeO<sub>2</sub> films on (110) NGO substrates showed lattice constant  
 5.395–5.41 Å, close to the standard 5.4 Å. The FWHM of the  
 peaks on the  $\theta/2\theta$  scans was significantly higher than the  
 size broadening, indicating strained or inhomogeneous layer  
 formation. Both YSZ and CeO<sub>2</sub> films showed wide rocking  
 curves (see Table II).

TABLE II. Typical structural properties of the films grown in standard epitaxial mode on low-angle TAS NGO. The spread of the presented parameters is ~50%. Actual film properties strongly depend on deposition conditions.

Film/substrate	Lattice mismatch <sup>a</sup> (%)	Lattice constant <sup>b</sup> (Å)	Strain $\Delta d/d$ (%)	FWHM of rocking curve (deg)	Film SICP inclination (deg)	Vicinal range (deg)
YSZ/NGO	+5.7– + 5.8	5.149	0.25	1.1	<0.5	2
CeO <sub>2</sub> /NGO	+1.0– + 1.1	5.405	0.15	0.5	<0.15	1
YBa <sub>2</sub> Cu <sub>3</sub> O <sub>x</sub> /CeO <sub>2</sub>	– 0.75– + 1.0	11.685	0.4	0.35	<0.1	1
BaZrO <sub>3</sub> /NGO	– 8.7– – 8.8	4.200	0.6	0.5	<0.1	no data

<sup>a</sup>Negative value corresponds to compressive strain, positive to tensile strain.

<sup>b</sup>Normal to substrate plane.

373 BZO films were deposited at the same conditions as fluorite  
 374 films. The deposition rate for BZO was  $0.225 \text{ \AA/pulse} =$   
 375  $0.45 \text{ \AA/s}$ . The BZO films showed good lattice perfection as  
 376 determined by XRD  $\theta/2\theta$  scans and rocking curves (Table II).  
 377 The lattice constant was  $4.197\text{--}4.213 \text{ \AA}$ , in good agreement  
 378 with the bulk value ( $\sim 4.2 \text{ \AA}$ ).

379 The YBCO thin films deposition parameters  
 380 ( $1.2\text{--}1.5 \text{ J/cm}^2$ , oxygen partial pressure 0.16 mbar, total  
 381 pressure of Ar/O<sub>2</sub> mixture 0.8 mbar) were optimized to  
 382 obtain the best superconducting and structural properties  
 383 for the films grown on the standard (110) NGO substrates.  
 384 Relatively low deposition temperature of  $730\text{--}750 \text{ }^\circ\text{C}$   
 385 suppressed the chemical interaction of YBCO with CeO<sub>2</sub>  
 386 bottom layer in multilayer structures. The deposition rate of  
 387  $0.8 \text{ \AA/pulse}$  ( $1.6 \text{ \AA/s}$  at standard 2 Hz laser pulse repetition  
 388 rate) provided enough time for relaxation of the deposited  
 389 material on the surface of the growing film. A prebake step  
 390 before deposition saturated the substrate surface with oxygen  
 391 and decreased the probability of chemical interaction with  
 392 the growing film. As a consequence, the lattice perfection  
 393 of the film significantly increased, especially for the thin  
 394 layer near the interface with the substrate [26], and both  
 395 size and density of the particles on the thin film surface  
 396 decreased. Post-deposition annealing was performed at  
 397  $450 \text{ }^\circ\text{C}$  in 800 mbar of oxygen for 1 h. All YBCO films  
 398 showed  $T_c$  above 89 K and a narrow superconducting  
 399 transition, proving good uniformity of the film structure.  
 400 The  $c$  lattice constant for all films was  $11.67\text{--}11.7 \text{ \AA}$ ,  
 401 confirming good reproducibility of the film fabrication  
 402 procedure. Rocking curve width, FWHM of the peaks of the  
 403  $\theta/2\theta$  scans, and strain estimation, depended on tilt angle,  
 404 underlying material, and deposition conditions, and varied  
 405 significantly.

406 Multilayers were usually prepared *ex situ* to have a  
 407 possibility to study the bottom layer properties before  
 408 and after deposition of the top layer. Some multilayer  
 409 structures were fabricated *in situ*, their parameters were  
 410 compared with that of corresponding *ex situ* fabricated  
 411 heterostructures.

412 Deposition rate of the deposited materials was calibrated  
 413 using selective wet chemical etching of grown films or with  
 414 lift-off removal of some part of the fabricated layer using  
 415 a predeposited and patterned hard mask. The value calcu-  
 416 lated using a number of pulses on target and calibrated  
 417 deposition rate we call the *nominal* thickness. Actual film  
 418 thickness may differ from the nominal value not only as a  
 419 result of small deviations of deposition parameters, but also  
 420 due to modification of the target surface by laser irradiation,  
 421 usually resulting in a lower ablation rate with time.  
 422 The thickness was also evaluated using the Williamson-Hall  
 423 method, the result was in good agreement with the nominal  
 424 value (error below 15%). Application of the Williamson-Hall  
 425 calculation allowed also determination of the variation of  
 426 the diffraction period normal to the diffraction plane  $\Delta d/d$ .  
 427 This parameter, usually called “strain,” was determined for  
 428 films of all materials if more than one diffraction peak was  
 429 present on the  $\theta/2\theta$  scan. Note that this is not the strain  
 430 related to the film-substrate lattice mismatch (Table I), though  
 431 sometimes a relation can be established between these two  
 432 parameters.

### III. RESULTS

433

434 The studies of epitaxial growth in semiconductor het-  
 435 erostructures showed that the tilt axis acts as an anchor setting  
 436 the initial epitaxial relation along the habit plane. Similarly, in  
 437 our previous studies [19–21] the (100) axes of the perovskite  
 438 films and the (110) axes of the fluorite films were parallel to  
 439 the substrate tilt axis [001] NGO for all deposition conditions.  
 440 In this study we assumed that this epitaxial relation remains  
 441 correct and limited the XRD studies to  $\theta/2\theta$  and  $\omega$  scans  
 442 around the substrate tilt axis with an initial offset angle  $\omega_0$ .  
 443 Our assumption is corroborated by similar integral intensity of  
 444 the XRD peaks for the films with the same nominal thickness.  
 445 When the observed peak integral intensity was significantly  
 446 smaller, we performed a search for additional orientations. All  
 447 orientations found still followed the same epitaxial relation  
 448 with some of the film axes parallel to the substrate tilt axis.

449 To avoid misunderstanding we will use the following nota-  
 450 tions:

- 451 (i) the substrate plane is the plane of substrate surface;
- 452 (ii) the tilt angle  $\gamma$  is the angle between the SICIP of film  
 453 or substrate (habit plane) and the substrate plane;
- 454 (iii) the inclination angle is the angle between the SICPs  
 455 of the substrate and the film;
- 456 (iv) the misorientation is the spread of orientations of  
 457 individual grains of the film around the main orientation,  
 458 usually determined as FWHM of the corresponding rocking  
 459 curve.

#### A. Standard epitaxial growth

460

461 The epitaxial growth for very small tilt angles (vicinal  
 462 range) does not differ much from growth on a substrate  
 463 ideally oriented along the habit plane. In fact, the surface  
 464 of a substrate exactly oriented along the habit plane usually  
 465 consists of local areas with very small tilt from the habit  
 466 plane: only the average orientation corresponds to the SICIP  
 467 (see, for example, discussion of different effects of roughness  
 468 in [11]). In our case morphological, structural, and electrical  
 469 parameters of the films remain the same as for the (110) NGO  
 470 substrate until some threshold tilt value; this angle determines  
 471 the vicinal range of epitaxy. Usually in this range the tilt of  
 472 the film due to the 3DGE growth hardly can be distinguished  
 473 from the tilt due to other mechanisms, taking into account  
 474 the accuracy of the XRD measurement and relatively high  
 475 misorientation of the film grains after PLD. Morphologically  
 476 the surface of the film shows no specific directions and the  
 477 grains are rounded or evenly oriented, if elongated.

478 At the same time, the films obtained in the vicinal range  
 479 with the “standard” epitaxial growth mode may be considered  
 480 as a reference for the 3DGE grown films at higher tilt angles.  
 481 For this reason in this section we present the main paramet-  
 482 ers of all films deposited on TAS of the vicinal range (see  
 483 Table II).

484 Generally we note that the parameters of the films grown in  
 485 the vicinal range depend on conformity of the lattice structure  
 486 and the mismatch strain introduced by the substrate. The  
 487 fluorite films deposited on the perovskite substrates show  
 488 a wider rocking curve and higher deviation of the average  
 489 orientation from the (110) NGO plane compared with the  
 490 perovskite films, but much lower variation of the out-of-plane

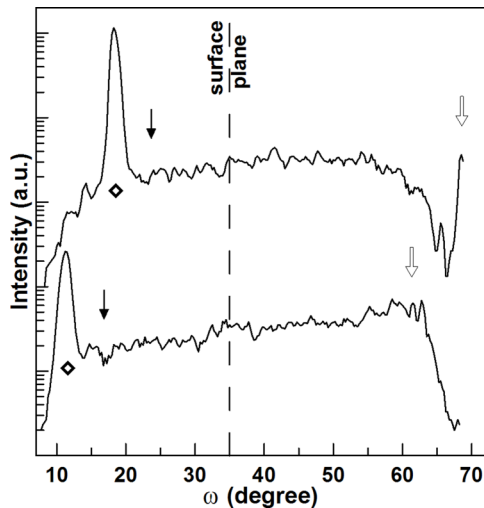


FIG. 3. Rocking curves for the (400) peak of CeO<sub>2</sub> films on TAS NGO. Substrate tilt angle: top curve 11.4°, bottom curve 18.4°. Black arrows show the angular position of the (110) NGO plane, white arrows correspond to the angular position of the (010) NGO plane. The 3DGE peaks of CeO<sub>2</sub> films are marked with diamonds.

YBCO deposition on perovskite substrates (see, e.g., [3], and [19–21,27]).

In our previous studies we assumed that a difference in the lattice structure is an important condition of 3DGE growth: a perovskite film on a perovskite substrate (like YBCO on NGO) and a fluorite film on a fluorite underlying layer would follow standard epitaxial growth mode. In fact, this is not true, as we will show below.

### B. 3DGE growth

#### 1. CeO<sub>2</sub> on NGO TAS

Typical rocking curves of CeO<sub>2</sub> films deposited by PLD on TAS NGO are presented in Fig. 3. The 3DGE peak is shifted from the position of the (110) NGO plane towards higher tilt angles, and the shift increases with substrate tilt angle. All our results for 3DGE growth of CeO<sub>2</sub> at different substrate tilt angles are gathered in Fig. 4(a). The film orientation dependence on substrate tilt is finely described by the simple geometrical model (1) until ~20°. Above this value the film tilt decreases towards the standard epitaxial relation (001) CeO<sub>2</sub> || (110) NGO. For substrate tilt angles 30°–35° we observed (110)-oriented CeO<sub>2</sub> films, with wide rocking curves (up to 4°) and high strain ( $\Delta d/d \approx 1^\circ$ ). These results are in good agreement with [18] and limitations of the simple geometrical model (3). Detailed description of deposition technique, (110)-oriented CeO<sub>2</sub> films properties, and specific cases in the angular range 30°–45°, will be presented in another publication. The CeO<sub>2</sub> film orientation for the tilt angles 25°–30° remains unclear: we could not reliably detect weak high-index XRD peaks from the CeO<sub>2</sub> film. Formation of a polycrystalline film seems probable, maybe with a set of predominant orientations.

lattice constant  $\Delta d/d$ . Both for fluorite and perovskite films the structural parameters are better for the materials with smaller lattice mismatch.

Deposition of YBCO on NGO TAS in all conditions and for all tilt angles resulted in standard epitaxial growth with relations  $\langle 100 \rangle (001) \text{ YBCO} || [001] (110) \text{ NGO}$ . The details of these films structure, morphology, and superconducting properties can be found in [21,27]. Such preservation of standard growth mode on TAS of all angles is considered as usual for

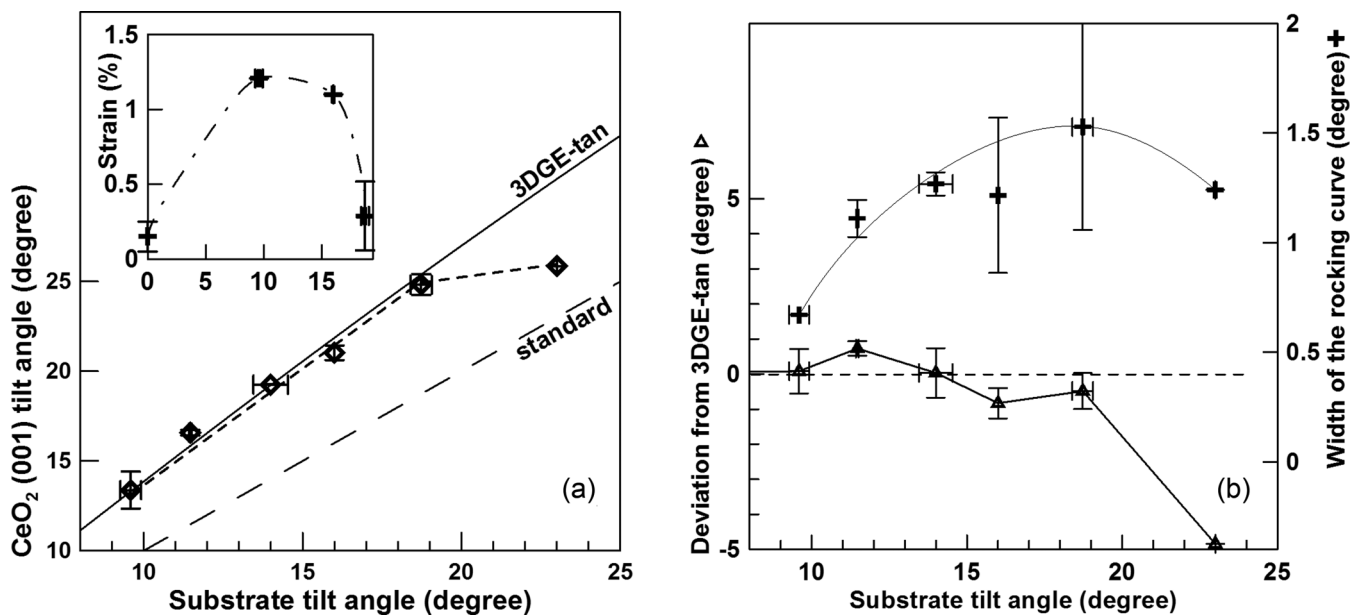


FIG. 4. Orientational relations of CeO<sub>2</sub> films on TAS NGO. (a) The film orientation follows the 3DGE-tangent growth mode [Eq. (1)] until 20°, and then the film tilt deviates towards the standard growth mode. Inset: Dependence of the lattice constant variation (strain) on the substrate tilt angle. (b) Deviation from calculated tilt angle (triangles) changes from small positive to small negative with substrate tilt angle until threshold at 20°. The width of rocking curve (crosses) increases with angle. Lines are given as guides for the eye.



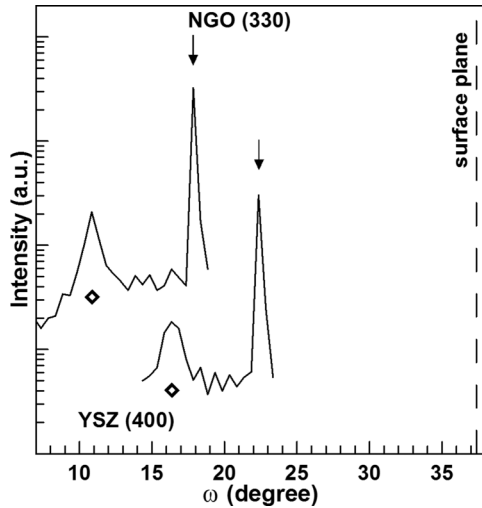


FIG. 5. Rocking curves for the (400) peak of the YSZ films on TAS NGO. Substrate tilt angle: top curve 19.5°, bottom curve 15.4°. Arrows show the angular position of the (110) NGO plane, the 3DGE (400) YSZ peaks are marked with diamonds.

spread of the FWHM's from sample to sample, increased [see Fig. 4(b), top curve]. When the growth mechanism turns towards the standard mode ( $\gamma = 23^\circ$ ), the width of the rocking curves decreases.

The lattice constant of the CeO<sub>2</sub> 3DGE films on TAS is close to that of the films on (110) NGO substrate, 5.399–5.408 Å. The strain and the FWHM of the rocking curves for the majority of the 3DGE films are significantly higher ( $\sim 1\%$  and  $\sim 1.3^\circ$ ) than that of the standard films ( $\sim 0.15\%$  and  $\sim 0.5^\circ$ , see Table II). The FWHM of the peaks on the  $\theta/2\theta$  scans is higher than expected on the size evaluation, implying significant inhomogeneity of the films similarly to the standard-oriented films grown on (110) NGO. Small deviations from optimal deposition conditions influences the 3DGE films properties in the same way as that of the standard films: the lattice constant increased and the strain in the film decreased with a decrease of the oxygen partial pressure during deposition. The rocking curve width showed no dependence on deposition conditions in the studied range.

2. YSZ on NGO TAS

The typical rocking curves of the YSZ thin films on TAS NGO are shown in Fig. 5. The Bragg diffraction angle for the (400) peak of YSZ is very close to that of the (330) peak of the NGO substrate, so a single measurement allows determination of angular positions of both substrate and film SICPs.

Typical dependence of the YSZ film orientation on substrate tilt angle is shown in Fig. 6(a). The tilt of the (100) plane of YSZ follows the geometrical model, sine variant (2), exceeding the calculated value in the angular range 5°–12°. The deviation from the 3DGE model is much higher than for CeO<sub>2</sub> 3DGE films, reaching +3° for substrate tilt angles

The deviation of the film orientation from the calculated value depends on film properties and deposition parameters. On average, the 3DGE film shows tilt angle slightly ( $< 1^\circ$ ) higher than calculated for tilt angles below 14°, and slightly ( $< 1^\circ$ ) smaller for tilt angles above this threshold, with a rapid increase of deviation when the film stops following pure-3DGE growth mode for tilt above 20° [Fig. 4(b)]. The misorientation of CeO<sub>2</sub> grains was tested using the XRD rocking curves measurements. For an increase of  $\gamma$  from 0° to 19° the FWHM of the rocking curves, as well as

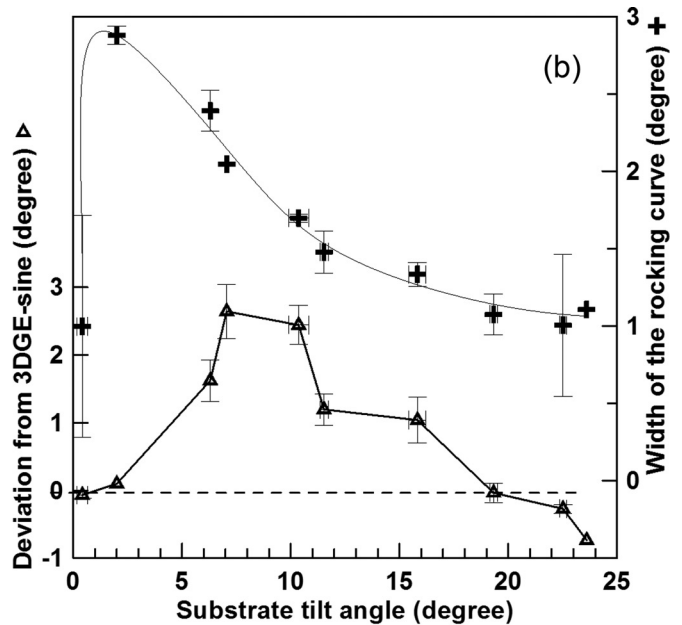
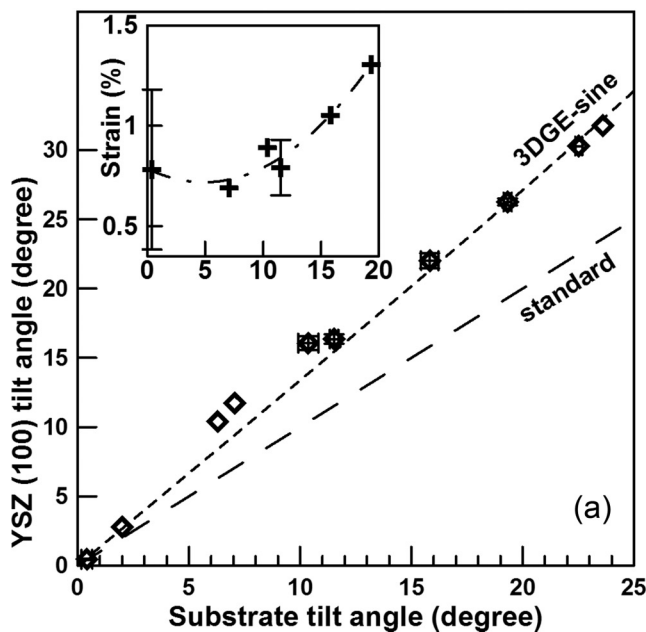


FIG. 6. Orientational relations of YSZ films on TAS NGO. (a) The film orientation follows the 3DGE-sine growth mode [Eq. (2)] at high substrate tilt angles and slightly exceeds the calculated value for 5°–12°. Inset: Dependence of the strain in the film on the substrate tilt angle. (b) Deviation from calculated tilt angle (3DGE-sine model, triangles) shows maximum in the 7°–10° range, correlating with the width of the rocking curve dependence on tilt angle (crosses). Lines are given as guides for the eye.

7°–10° [Fig. 6(b), bottom curve], but similarly decreases with tilt angle, finally changing to negative values for tilt angles above 20°. The FWHM of the rocking curve for the YSZ films deposited at tilt angles close to zero shows a very high spread from sample to sample [Fig. 6(b), top curve]. A change of the substrate tilt angle to ~2° results in a huge rise of the grains misorientation (the FWHM increases to ~3°). The further increase of the substrate tilt angle results in a gradual decrease of FWHM with saturation at ~1° at high tilt angles.

The variation of the lattice parameter  $\Delta d/d$  also shows a very high spread from sample to sample at zero tilt angle [see inset Fig. 6(a)]. Until 12° it remains almost constant, and increases only above 15°, when the deviation from the calculated angle becomes small and the width of the rocking curve saturates [Fig. 6(b)]. The strain and the width of the rocking curve show clear anticorrelation.

The lattice constant of the YSZ films varied from 5.134 to 5.157 Å (5.148 Å average, the measurement accuracy was low, ~0.007 Å), independently on the substrate tilt angle. The deposition of YSZ films seem to be rather reproducible, no significant changes in film orientation and structure could be observed with small changes of deposition conditions. An increase of thickness of the YSZ film (100 to 900 Å) leads to a decrease of strain and a decrease of the rocking curve width: with an increase of film thickness the film becomes more homogeneous and more aligned.

### 3. BaZrO<sub>3</sub> on NGO TAS

The expected growth mode of a perovskite BZO film on a perovskite NGO substrate was standard, and for high (24°) tilt angles this assumption proved to be correct. Surprisingly, at a substrate tilt angle of 10° the film orientation showed excellent agreement with the geometrical model (Fig. 7). The discrepancy from the calculated value (tangent model) is less than 0.05°, and deviation from the standard orientational relations exceeds 0.8°. The width of the rocking curve increased for high tilt angle (see inset Fig. 7), similarly to the CeO<sub>2</sub> 3DGE films [Fig. 4(b)]. The strain in the films decreased with tilt angle, anticorrelating to the rocking curve width. The measured lattice constant was 4.199 Å, in good agreement with the standard 4.2 Å value, and did not depend on tilt angle.

### C. 3DGE growth in multilayer heterostructures

All studied multilayer heterostructures on NGO TAS showed 3DGE growth through the whole thickness of the heterostructure, except when a chemical reaction took place between the neighboring layers (YBCO over CeO<sub>2</sub>, YSZ, or BZO). Even in these cases some part of the upper layer showed 3DGE growth, especially at lowered deposition temperatures.

#### 1. CeO<sub>2</sub>/YSZ/NGO

A thin (20–100 Å) CeO<sub>2</sub> layer is often introduced between the YSZ bottom layer and YBCO top layer to prevent chemical interaction. A weak signal from the thin CeO<sub>2</sub> layer is hard to distinguish from a strong neighboring YSZ peak, especially at small tilt angles. Still for some samples we managed to determine the mutual orientation of the films in

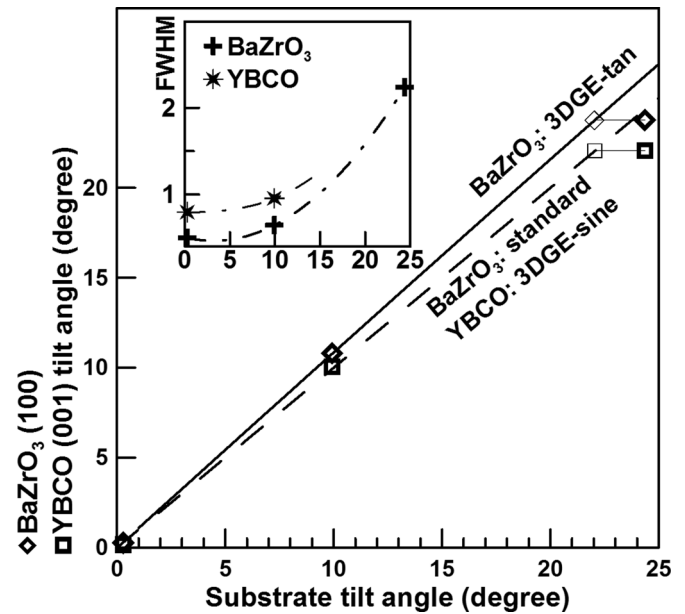


FIG. 7. Orientational relations in the YBCO/BZO heterostructures on TAS NGO. Diamonds: BZO, squares: 3DGE part of the YBCO films. Thin symbols: Calculated positions if BZO kept 3DGE growth mode to 24°. Inset: Dependence of the width of the rocking curve of the BZO (200) peak (crosses) and YBCO (005) peak (stars) on the substrate tilt angle. The lines on the inset are guides for the eye.

a YBCO/CeO<sub>2</sub>(75 Å)/YSZ trilayer on NGO TAS (Fig. 8). We expected standard epitaxial growth of a fluorite CeO<sub>2</sub> film over a fluorite YSZ bottom layer, with strictly parallel (100) planes in both layers. Instead, the 3DGE growth was observed not only for the fluorite YSZ layer over the perovskite NGO substrate, but also for the CeO<sub>2</sub> film over the heterostructure (Fig. 8). The tilt angle for the CeO<sub>2</sub> layer is higher than that of the YSZ layer, in agreement with greater lattice constant (5.4

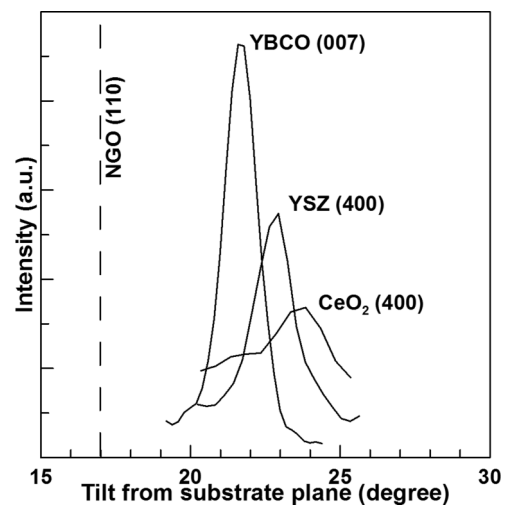


FIG. 8. Rocking curves of the (400) YSZ, (400) CeO<sub>2</sub>, and (007) YBCO peaks of the trilayer YBCO/CeO<sub>2</sub>/YSZ heterostructure on TAS NGO. The substrate tilt angle is 16.9°. All layers follow the 3DGE growth mode.

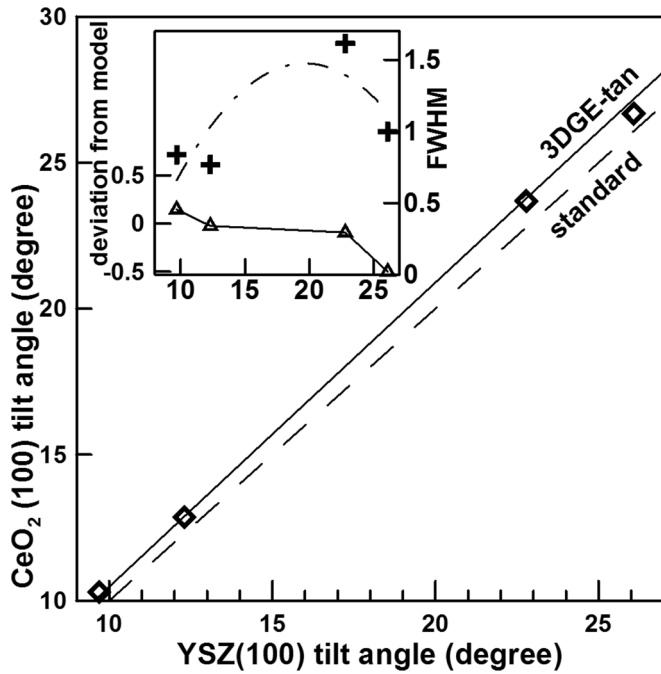


FIG. 9. Orientation of CeO<sub>2</sub> films on 3DGE YSZ layers on TAS NGO. Inset: Dependence of the deviation from the 3DGE-tangent model (triangles) and the width of the rocking curve of the CeO<sub>2</sub> (400) peak (crosses) on the substrate tilt angle. The lines are guides for the eye.

and 5.15 Å). The calculated and measured tilt angles match well (Fig. 9). The tangent model (1) describes the angular behavior better than the sine model (2), calculations are done taking into account an excessive tilt of the YSZ layer for tilt angles 5°–12° [Fig. 6(a)]. Similar to the CeO<sub>2</sub> films on bare NGO TAS the deviation from calculated value changes from positive to negative at ~12° tilt of the underlying layer [compare Fig. 4(b) and inset Fig. 9]. At high tilts (above 23° for CeO<sub>2</sub>/YSZ) a deviation towards the standard growth mode is observed [Figs. 9 and 4(a)]. The width of the rocking curve increases with tilt angle, but drops when the tilt changes towards the standard orientation. We may conclude that all orientational features of the 3DGE tangent mode growth of CeO<sub>2</sub> on TAS NGO are preserved on tilted-axes YSZ bottom layer.

The measured lattice constant of the CeO<sub>2</sub> interlayer is  $5.397 \pm 0.009$  Å, somewhat smaller than the standard 5.4 Å value, or  $5.404 \pm 0.004$  Å typical for CeO<sub>2</sub> grown on NGO TAS at the same deposition conditions. Incorporation of Zr atoms into the CeO<sub>2</sub> growing film may be the reason for this difference.

## 2. YBCO/CeO<sub>2</sub>/NGO

The YBCO grains on a CeO<sub>2</sub> layer showed either *c* orientation or 3DGE orientation; films with mixed orientation were observed most commonly. The orientation of the YBCO grains depended on tilt angle and deposition conditions, but the most affecting factors are the properties of the underlying CeO<sub>2</sub> layer, set by CeO<sub>2</sub> fabrication technique, and preparation of the CeO<sub>2</sub>/NGO sample to the YBCO film deposition.

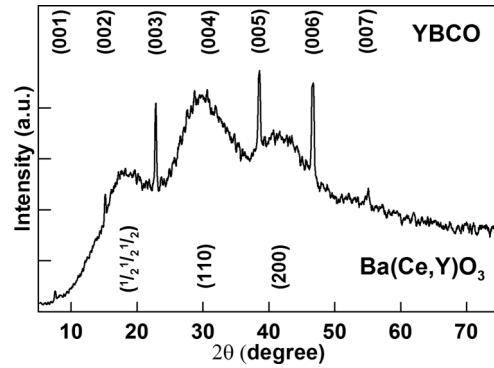


FIG. 10. X-ray  $\theta/2\theta$  scan of the YBCO/CeO<sub>2</sub>/NGO heterostructure along the substrate normal, nominal substrate tilt angle 22°. A set of broad peaks from polycrystalline Ba(Ce, Y)O<sub>3</sub> reaction layer can be detected on the scans, produced by small (5–15 Å) crystallites.

The mechanisms of *c*-oriented YBCO film formation over the CeO<sub>2</sub> layer are similar to the growth processes of YBCO films on the YSZ layers (see, e.g., [28,29]) and result from interaction of Ba with CeO<sub>2</sub> with formation of a Ba(Ce, Y)O<sub>3</sub> interlayer. An increase of thickness of such an interlayer leads to secondary seeding of Ba(Ce, Y)O<sub>3</sub> grains with orientations providing minimization of the surface energy. We observed (100), (110), and (111) orientations of Ba(Ce, Y)O<sub>3</sub> grains along the substrate plane (Fig. 10). The wide peaks in the angular range 10°–50° corresponded to very small (5–20 Å) crystallites with lattice constant ~4.31 Å. The YBCO films on the Ba(Ce, Y)O<sub>3</sub> interlayer always showed *c*-oriented growth (Fig. 10), sometimes mixed with the tilted grains.

The tilt angle of the tilted YBCO grains differed both from the substrate tilt angle and the tilt angle of the 3DGE CeO<sub>2</sub> layer (Fig. 8), and increased monotonously with the substrate tilt angle, implying the 3DGE or some similar growth mechanism [Fig. 11(a), solid diamonds]. This effect was noticed in [21], but no explanation was suggested. Assuming 3DGE growth with a step height equal to  $c/3 = 3.933$  Å (on the early stages of YBCO growth it tends to grow in the pseudocubic form), we get the YBCO tilt angle very close to that of the substrate (step height 3.864 Å), with a deviation below 1° in the whole possible range of tilt angles. The actual deviation from the substrate tilt angle is much higher [Fig. 11(a)].

The explanation for the 3DGE growth with the observed angles is also chemical interaction with formation of a very thin (not detected with XRD techniques) Ba(Ce, Y)O<sub>3</sub> layer between CeO<sub>2</sub> and YBCO films. This layer is strictly aligned with the underlying CeO<sub>2</sub> film, (100) Ba(Ce, Y)O<sub>3</sub> || (100) CeO<sub>2</sub>, and the tilt angle of the YBCO film is determined not by step height of CeO<sub>2</sub> layer but that of Ba(Ce, Y)O<sub>3</sub>. From the atomistic point of view we may assume chemical bonding of the surface CeO layer with the incoming Ba atoms, with formation of a half of a perovskite BaCeO<sub>3</sub> cell, providing out-of-plane lattice constant (and, consequently, terrace step height) corresponding to BaCeO<sub>3</sub>, not CeO<sub>2</sub>. We note that 1/2- or 1/3-lattice constant as the height of the surface step was already mentioned before [15,17]. The agreement with the 3DGE-sine model assuming BaCeO<sub>3</sub> step height (4.31 Å measured for small crystallites)

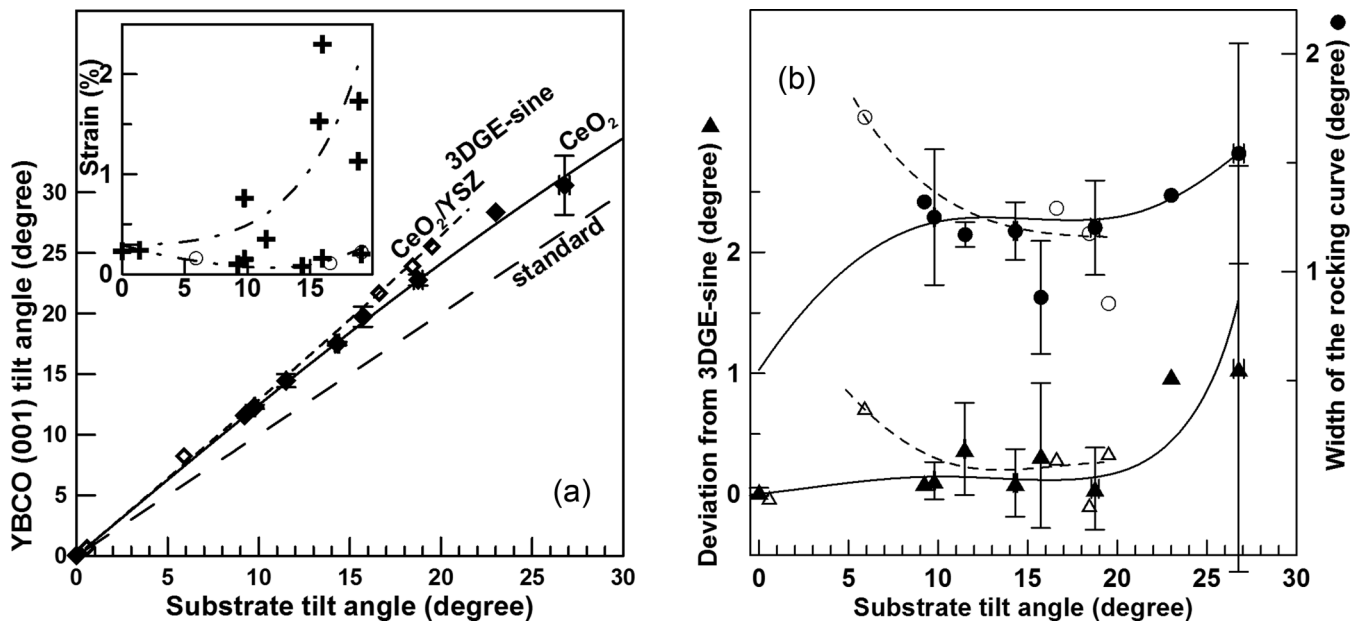


FIG. 11. Orientational relations of YBCO films on CeO<sub>2</sub> layers and on CeO<sub>2</sub>/YSZ bilayers on TAS NGO. (a) The YBCO film orientation follows the 3DGE-sine growth mode [Eq. (2)] both for films grown on a single CeO<sub>2</sub> layer (solid diamonds, solid line) and on CeO<sub>2</sub>/YSZ bilayers (open diamonds, short-dashed line). Inset: Dependence of the strain in the YBCO film on the substrate tilt angle, crosses: single CeO<sub>2</sub> layers, circles: CeO<sub>2</sub>/YSZ bilayers. (b) Absolute deviation from calculated tilt angle (3DGE-sine model, triangles) correlates with the width of the rocking curve (circles). Solid symbols correspond to the YBCO films on single CeO<sub>2</sub> layers, open symbols YBCO films on CeO<sub>2</sub>/YSZ bilayers. The lines are given as guides for the eye.

is impressive up to 27° [Fig. 11(a), solid diamonds]. Note that down-bending of the calculated dependence [solid line Fig. 11(a)] is determined by the tangent dependence of the tilt of the CeO<sub>2</sub> layer [Fig. 4(a)]. Measured data for the CeO<sub>2</sub> films at substrate tilt angles above 23° are absent, so the curve Fig. 11(a) in this range was calculated assuming tangent dependence for CeO<sub>2</sub> and sine formula for YBCO over the intermittent Ba(Ce, Y)O<sub>3</sub> layer.

The average deviation of the YBCO film orientation from the calculated value remained small ( $\sim 0.2^\circ$ ) until  $\sim 20^\circ$ , and rapidly increased for tilt angles above  $20^\circ$  [Fig. 11(b), solid triangles]. The FWHM of the rocking curves repeated this dependence [Fig. 11(b), solid circles]. The lattice constant  $c$  of the YBCO films was almost constant  $11.684 \pm 0.007 \text{ \AA}$  for all tilt angles below  $20^\circ$ . Precise determination of the lattice constants for higher angles was complicated due to the limitations of the applied asymmetric geometry of the x-ray diffraction. The strain  $\Delta d/d$  was estimated for the same angular range  $0^\circ$ – $20^\circ$ ; the films can be divided into two groups, with very low strain below 0.2%, and with strain increasing with tilt angle to 1% and more [see inset Fig. 11(a)]. The increasing dependence resembles strain behavior in the 3DGE YSZ films on TAS NGO.

### 3. YBCO/CeO<sub>2</sub>/YSZ/NGO

The trilayer YBCO/CeO<sub>2</sub>/YSZ structures were not studied extensively due to the low (30–80 Å) thickness chosen for the CeO<sub>2</sub> layers for the planned experiment. Still some samples allowed measurements for all three layers (Figs. 8 and 9).

The YBCO films on the CeO<sub>2</sub>/YSZ bilayer show the same orientational behavior as on the single CeO<sub>2</sub> layers:  $c$ -oriented, 3DGE-oriented, and mixed-orientation films were formed depending on conditions for the chemical reaction with formation of a Ba(Ce, Y)O<sub>3</sub> layer. The properties of the 3DGE grains are shown with open symbols in Fig. 11.

The tilt of the YBCO film [Fig. 11(a), open diamonds] is described by the same sine model as in the bilayer case. Introduction of the YSZ layer with sine 3DGE dependence below a CeO<sub>2</sub> layer with tangent dependence results in a significant difference ( $0.3^\circ$ – $1.0^\circ$ ) between the measured values in the high-angle range, clearly distinguished with the applied XRD techniques. The deviation from the calculated value is slightly higher than for the YBCO 3DGE films on a single CeO<sub>2</sub> layer [Fig. 11(b), open triangles], and increases at low tilt angles ( $5^\circ$ – $8^\circ$ ). Unfortunately, there is no available data for YBCO 3DGE films on a single layer for this angular range. The YSZ 3DGE films showed a similar increase of deviation for the  $5^\circ$ – $10^\circ$  range [Fig. 6(b)]. The width of the rocking curve correlated well with the absolute deviation value, similarly to the YBCO 3DGE films on a single CeO<sub>2</sub> layer [Fig. 11(b), closed symbols]. The FWHM of the rocking curve in the angular range  $15^\circ$ – $20^\circ$  does not differ much from the measured values for YBCO 3DGE films on a single CeO<sub>2</sub> layer.

The lattice constant of the 3DGE YBCO films on the CeO<sub>2</sub>/YSZ bilayers is the same as for the 3DGE YBCO films on single CeO<sub>2</sub> layers:  $11.684 \pm 0.005 \text{ \AA}$ , and also shows no angular dependence. The evaluated strain is low for all studied films, less than 0.25%, so all the YBCO films on bilayers belong to the low-strain group of samples [see inset Fig. 11(a)].



#### 4. YBCO/BaZrO<sub>3</sub>/NGO and YBCO/BaZrO<sub>3</sub>/YSZ/NGO

To prove YBCO growth mechanisms on BaCeO<sub>3</sub> we fabricated a set of samples on TAS NGO with a 80-nm-thick buffer layer of BaZrO<sub>3</sub> from an available commercial target. The mechanisms of growth of *c*-oriented YBCO films on ZrO<sub>2</sub> are very similar to the growth of *c*-oriented YBCO on CeO<sub>2</sub>, so we expected similarity also in case of 3DGE growth, if obtained on BZO.

The BZO films showed 3DGE behavior in the low-angle range 0°–10°, and a change to standard growth mode for high substrate tilt angle (24°, Fig. 7 diamonds). The YBCO films were growing in mixed orientation, with a *c*-oriented main part (>90%) and a 3DGE minor part (Fig. 7, squares). The step height of YBCO during growth is close to the lattice constant of NGO, so we expected back-rotation of the YBCO (001) plane towards the substrate plane and almost coincidence with the substrate (110) plane. This is exactly what we observed in experiment: agreement between the calculated and the measured values is better than 0.2° (Fig. 7, squares). The breach of the 3DGE growth mode of BZO at high tilt angles did not affect the 3DGE-sine growth mode of YBCO on BZO: assuming a tilt angle of BZO resulting from the 3DGE growth (thin diamond, Fig. 7) we get a position of the YBCO (001) plane exactly at the position calculated using 3DGE-sine model (thin square, Fig. 7).

To model the process of YBCO growth on CeO<sub>2</sub> we deposited YBCO/BZO heterostructures *in situ* on a 3DGE YSZ film on 16° TAS NGO. The result completely confirmed our predictions: the tilted part of the YBCO film (20.26° tilt) followed the 3DGE-sine model, with tilt angle of the bottom layer equal to that of the YSZ film (~22°), but with a step height equal to the lattice constant of BZO (4.2 Å). This means that at least part of the ~22.5-nm-thick BZO layer grows on the 3DGE YSZ film in the standard mode, (100) BZO|| (100) YSZ. With the available equipment we could not detect these standard-oriented BZO grains on the rocking curves, being out of the scan range.

The main part of the YBCO/BZO heterostructure showed the same properties as YBCO/Ba(Ce, Y)O<sub>3</sub> layer on 3DGE CeO<sub>2</sub> films. The main part of the BZO layer was growing (100), (110), and (111) oriented, with *c*-oriented YBCO growing over these grains. Some part of the BZO layer followed the 3DGE-sine growth mode on tilted YSZ layer with tilt angle of 19.28° (calculated value 19.35°). YBCO growth on these 3DGE BZO grains was not detected, neither in standard nor in 3DGE orientation.

## IV. DISCUSSION

The growth of films with significant tilt of SICP from habit planes of the tilted-axes substrate are usually considered as rare and, in some sense, exceptions from the general rule of standard growth mode. Our results show that, in fact, for all-metaloxide heterostructures the 3DGE growth mechanism is more common than standard, especially for the angular range below 20°.

### A. Epitaxial issues

To start discussing the 3DGE growth mechanism we should first revert to the question of epitaxy. In the very

beginning this term was used when the structure of the film repeated the structure of the substrate. Rigorously only the films of the same material as the substrate, but with different dopant or with different level of doping, may be considered *epitaxial*. This term sometimes was also used to describe heterostructures in which the material of the film had the same lattice structure as the substrate, and the lattice constants did not differ much. Later the term *epitaxy* was used when a strict relation could be established between crystallographic planes and directions of the film and crystallographic planes and directions of the substrate. These films were also known as *oriented* films. The orientational relations with the substrate for some of the oriented films were set by the atomic structure of the substrate surface, and this class of film inherited the name of epitaxial films, while the films for which some of the orientational relations are set by film surface retained the name of oriented films.

The films presented in this study show *no* parallelism between some SICPs in the film and in the substrate, only the tilt axis is bonding the film and substrate lattice in a strict way. At the same time, the general orientation of the film is set not by the *surface* of the film, but by the *microstructure* of the substrate surface. The changes of the microstructure, in particular, the distance between the edges of the terraces, result in a change of the film orientation, in agreement with a strict mathematical relation. From this point of view the films are epitaxial, not just oriented.

The term *graphoepitaxy*, if it had been suggested in the very beginning of the fabrication of epitaxial films, would have been considered as an oxymoron, something like a “dry liquid.” The orientation of the graphoepitaxial films was set not by the atomic structure of the substrate, but by the macroscopic structures of the surface of the substrate. Actually, the first graphoepitaxial films were fabricated from a material with totally different crystal structure from the structure of the substrate, making application of the term of “epitaxy” in the strict meaning absolutely impossible. Still the term settled, and at the moment the “graphoepitaxial” oriented films are fabricated, discussed, and categorized in different types (see, for example [30]).

Our films are (i) oriented and (ii) this orientation is set by the surface features of the substrate, i.e., they can be considered as graphoepitaxial. At the same time, the surface features that set the orientational relations are determined by the crystal structure of the substrate, and this makes our films epitaxial in the modern meaning of the term. Thus, the films grown by the 3DGE mechanism are epitaxial and graphoepitaxial at the same time.

We would like to emphasize a third point: the bonding of the lattices of the film and the substrate is realized in three orthogonal directions: the tilt axis, the length of the terrace, and the out-of-plane lattice constants set the orientational relations in a unique way. Moreover, the translational distances in all three directions are important for the film orientation, as well as matching (and mismatching) of these distances in the film and the substrate. This makes the discussed growth mechanism *essentially* three dimensional, and justifies the proposed name “three-dimensional graphoepitaxial,” 3DGE, mechanism.

## B. Growth modes and models

882

883 Disregarding the complicated microstructural mechanisms  
884 of formation of tilt in the films on TAS [11–13], we may  
885 identify two simplified mechanisms of formation of the 3DGE  
886 films: the overgrowth mechanism [15], and the simultaneous  
887 seeding mechanism [16].

888 The first one suggests seeding of the film near the edge-  
889 terrace joints, and growth of these from the terrace edge.  
890 When the growing layer reaches the end of the terrace, it  
891 encounters a different height of the surface that it should  
892 overgrow, and accommodates this difference [Fig. 1(b)]. The  
893 resulting angle depends on the length of the terrace  $d_t$  and  
894 simple considerations result in the tangent model (1). This  
895 growth mode corresponds to the graphoepitaxy of cases 2 and  
896 3 in Fig. 1(b) in [30].

897 The second simplified model implies simultaneous seeding  
898 of the film on neighboring “seeding knots” in the edge-terrace  
899 joints [Fig. 1(c)]. In this case orientation of the film is formed  
900 in the same way as for the standard growth mode, because  
901 the seeding knots mimic the atom position in the atom-on-  
902 atom epitaxial growth. The tilt angle of the film depends on  
903 the distance between the seeding knots  $d_s$ , and the resulting  
904 model follows a sine dependence (2).

905 The two models hardly can be distinguished at tilt angles  
906 below  $10^\circ$ , so previous studies never faced a necessity to  
907 choose between these two mechanisms.

908 The first model seems to be more probable for small tilt  
909 angles, because the lattice of the growing layer should settle  
910 well before overgrowth would change the tilt angle. The  
911 demand to “settle” the structure of the growing layer means  
912 that at high angles this mechanism is improbable. Assuming  
913 two unit cells as a smallest “settled” seed, we get the limit for  
914 the tangent mode growth:

$$\gamma_t < \arctan[c_s/(2a_f)], \quad (4)$$

915 where  $a_f$  is the film unit cell size along the growth direction.

916 For  $\text{CeO}_2$  growth on NGO this formula gives  $\gamma_t = 19.7^\circ$ ,  
917 and, indeed, at angles above  $20^\circ$  the  $\text{CeO}_2$  film deviates  
918 towards the standard growth mode [Fig. 4(a)].  $\text{CeO}_2$  depo-  
919 sition on YSZ formula (4) gives  $25.5^\circ$ , and the observed  
920 deviation starts at  $24^\circ$ – $25^\circ$  (Fig. 9). The change of the growth  
921 mechanism to standard for BZO on NGO at  $24^\circ$  (Fig. 7,  
922 diamonds) also may be a result of limited angular range of  
923 the tangent growth mode ( $\gamma_t = 24.7^\circ$ ). For YSZ on NGO the  
924 limiting angle is  $20.6^\circ$ , but we cannot see a distinct trend  
925 towards standard growth mode even for  $\sim 23.5^\circ$ . Note that the  
926 sine model provides a better fit for 3DGE growth of YSZ.  
927 Similarly no pronounced deviation towards standard growth  
928 at high angles was observed for YBCO on  $\text{CeO}_2$ , another pair  
929 of materials better described by the sine formula (Fig. 11).

930 The second simplified mechanism, simultaneous seeding,  
931 to the contrary, is promoted by a small distance between the  
932 seeding knots, and would be favorable at high tilt angles. At  
933 small tilt angles the seeding would be more efficient for closer  
934 placed seeding knots, so, taking into account a certain spread  
935 of the distance  $d_s$  along the substrate surface, we may expect  
936 slightly higher average tilt angles compared to the calculated  
937 value. This is exactly what happens for YSZ on NGO (Fig. 6),  
938 and for YBCO on  $\text{CeO}_2$  [Fig. 11(b), open triangles].

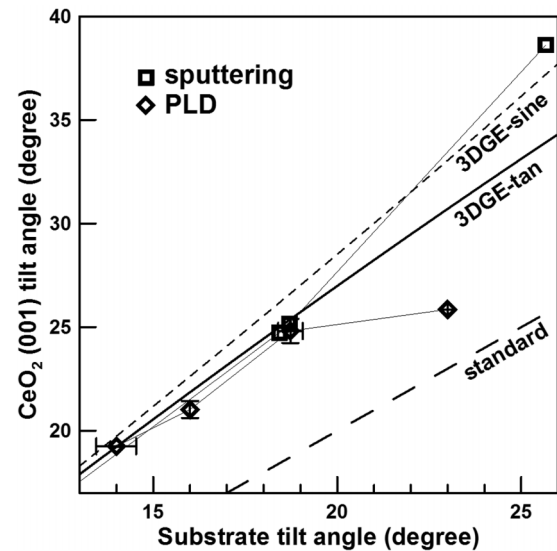


FIG. 12. Comparison of tilt of  $\text{CeO}_2$  films on NGO TAS deposited by PLD (diamonds) and rf sputtering (squares, [19,20]) at high substrate tilt angles.

939 Do we really observe two different 3DGE growth modes,  
940 or is it just a measurement error? The data in Fig. 11(a) seem  
941 to prove the presence of two different modes: the YBCO films  
942 on a single  $\text{CeO}_2$  layer and on a  $\text{CeO}_2$ /YSZ bilayer show dif-  
943 ferent angular dependence in the range  $15^\circ$ – $20^\circ$  because a sin-  
944 gle  $\text{CeO}_2$  layer fabricated by PLD follows the tangent mode,  
945 while a YSZ layer below  $\text{CeO}_2$  demonstrates sine dependence.  
946 Comparison of  $\text{CeO}_2$  films fabricated by different techniques  
947 also seem to prove the existence of two different growth  
948 modes (Fig. 12): the tilt of the PLD films at angles above  $20^\circ$   
949 downturns towards the standard growth mode, while for the  
950 films deposited with sputtering techniques [19,20] the tilt still  
951 follows the 3DGE mechanism, sine dependence.

952 The data on growth modes for different film-substrate  
953 combinations are gathered in Table III. We could not unam-  
954 biguously determine the factors that promote the overgrowth  
955 mechanism or the simultaneous seeding mechanism. Still, as  
956 much as we may conclude from the data in Table III, the com-  
957 pressive strain promotes the overgrowth mechanism, while  
958 films with tensile strain introduced by the underlying layer  
959 tend to follow the simultaneous seeding mode. Compressive  
960 strain, in the case of cubic film and substrate lattices, and  
961 equality of step height and lattice constant, corresponds to  
962  $c_f > c_s$  and increased tilt angle of the top layer compared to  
963 the tilt angle of the bottom layer. Tensile strain, with the same  
964 assumptions, corresponds to a decreased tilt angle of the top  
965 layer, so the tangent mode seems to be typical for the increase  
966 of the tilt angle due to the 3DGE growth mechanism, while the  
967 sine mode for the decrease of the tilt angle. This is not so for  
968 more complicated film-substrate matching, like YSZ/NGO,  
969 when tensile strain (and simultaneous seeding mechanism) is  
970 introduced into the film due to the  $45^\circ$  axes tilt in the habit  
971 plane (110) NGO, but the film tilt angle  $\gamma'$  increases because  
972 the step height of YSZ is higher than that of NGO (Fig. 6).

973 The dependencies of the critical parameters on the lattice  
974 mismatch seem to confirm this observation: for example,

TABLE III. Observation of sine and tangent growth modes for different film-substrate combinations.

Film/substrate	Lattice mismatch <sup>a</sup> (%)	Growth mode	$\gamma_t$ , measured/calculated (deg)	Excessive tilt, value/range (deg)	Comment
BZO/NGO	-8.7- - 8.8	tangent <sup>b</sup>	(<24)/24.7	n/a	
CeO <sub>2</sub> /YSZ	-5.0	tangent	~24.5/25.5	n/a	
CeO <sub>2</sub> /NGO	+1.0- + 1.1	tangent	20/19.7	n/a	by PLD
		sine	n/a	no data	by rf sputtering
YBCO/CeO <sub>2</sub>	-1.8- - 0.1	sine	n/a	0.7/6	
YSZ/NGO	+5.7- + 5.8	sine	n/a	2.5/(6-10)	
YBCO/BZO	+7.4- + 8.9	sine <sup>b</sup>	n/a	(0.03/10)	
Ba(Y, Zr)O <sub>3</sub> /YSZ	+11.5 <sup>c</sup>	sine <sup>b</sup>	n/a	no data	

<sup>a</sup>Positive value corresponds to tensile strain, negative to compressive strain.

<sup>b</sup>Insufficient data for a reliable conclusion.

<sup>c</sup>No 45° in-plane rotation.

the deviation towards the standard mode for the overgrowth mechanism seems to start at smaller angles for higher compressive strain, as seen from the BZO/NGO, CeO<sub>2</sub>/YSZ, and the CeO<sub>2</sub>/NGO pairs. The excessive tilt at small tilt angles seems to increase with an increase of the tensile lattice mismatch, when we compare the YBCO/CeO<sub>2</sub> and YSZ/NGO combinations (Table III).

Two rows of Table III with small mismatches ~1% contradict to this suggested rule: YBCO/CeO<sub>2</sub> (small compressive strain, sine dependence) and CeO<sub>2</sub>/NGO (small tensile strain, tangent dependence). If we suppose that the CeO<sub>2</sub> lattice constant is ~1.5% higher than measured, we remove this discrepancy: the lattice mismatch for CeO<sub>2</sub>/NGO becomes weakly compressive (~ -0.5%), and for YBCO/CeO<sub>2</sub>, weakly tensile (~ +0.6%), in good agreement with the other data. The thermal expansion coefficients cannot account for such corrections, being almost the same for all three materials [NGO : (4.5-9.0) × 10<sup>-6</sup> K<sup>-1</sup> from different references, CeO<sub>2</sub> : (8.5-9.5) × 10<sup>-6</sup> K<sup>-1</sup>, and YBCO : (11-13) × 10<sup>-6</sup> K<sup>-1</sup>]. The increase of the CeO<sub>2</sub> lattice constant during deposition can happen as a result of incomplete oxygenation (see discussion of oxygen removal from and incorporation to, for example, in [31]), and 1.5% is not the highest possible expansion. The missing oxygen could be incorporated into the CeO<sub>2</sub> layer immediately after the deposition, shrinking the lattice constant to the observed value.

For CeO<sub>2</sub>/NGO both mechanisms were observed for different deposition techniques. We note that for e-beam evaporation and rf sputtering the deposition rate is small, so the CeO<sub>2</sub> film grows completely oxygenated, while for PLD a certain amount of oxygen vacancies is generated in the growing film, expanding the CeO<sub>2</sub> lattice. Tensile strain for the completely oxygenated CeO<sub>2</sub> films would account for sine mode for the e-beam evaporated and rf-sputtered films, while an increase of lattice constant by more than 1% during PLD would result in a compressive strain and tangent growth mode.

### C. Orientational features

The width of the rocking curve is a parameter that sheds light on the peculiarities of the 3DGE film formation. The misorientation of the grains strongly depends on the seeding mechanism, and differences in rocking curve width depen-

dence on angle imply formation of 3DGE films in different ways.

A comparison of properties of CeO<sub>2</sub> films on NGO TAS [Fig. 4(b)] and on YSZ 3DGE layers on NGO TAS (inset Fig. 9) show clear similarities. The deviation from the calculated curve slowly decreases from small-positive to small-negative values until the threshold angle  $\gamma_t$ , when negative deviation rapidly increases. This dependence is accompanied by an increase of the width of the rocking curve until the same threshold angle, after which it drops to smaller level. Both sets of data can be brought to the same scale by plotting the dependence on the film tilt angle instead of using the substrate tilt angle, and by normalizing the deviation from the calculated value by division on the inclination ( $\gamma' - \gamma$ ) due to the 3DGE growth mechanism. This transformation makes visible the identity of the two dependencies [Fig. 13(a)]. Unfortunately, we have not enough data in the range 0°-10° to present the complete dependence of the deviation from the geometrical model (1).

The reasons for the misorientation of the grains of the film were presented in [15]. The terraces on the substrate surface are not equal, so a certain spread of the orientation of the grains after overgrowth of the next step is present from the beginning, and strongly depends on the size of the grains of the film. If the grains are smaller than the typical terrace length  $d_t$ , the grains would grow following the standard growth mode. This effect is clearly demonstrated in [17], where the change of the growth mode to standard at low deposition temperature is a result of a decrease of the size of the CeO<sub>2</sub> grains. The combination of a distribution of size of the grains and a distribution of the length of the terraces results in a distribution of the orientation of the grains starting from the standard mode and until film tilt angles exceeds the calculated  $\gamma_t$  using the geometrical model. The spread of the orientation of the grains will increase when step bunching starts on the substrate surface, with formation of steps with height 2, 3, and more times the ordinary height  $c_s$ . For the typical perovskite substrates step bunching starts at ~10°, depending on preparation conditions [5], and we observe an increase of the width of the rocking curve at ~13° [Fig. 13(a)]. The rapid decrease of the film tilt angle towards the standard relations at angles above the threshold  $\gamma_t$  may be a result of very small lengths of terraces, so that the overgrowth happens

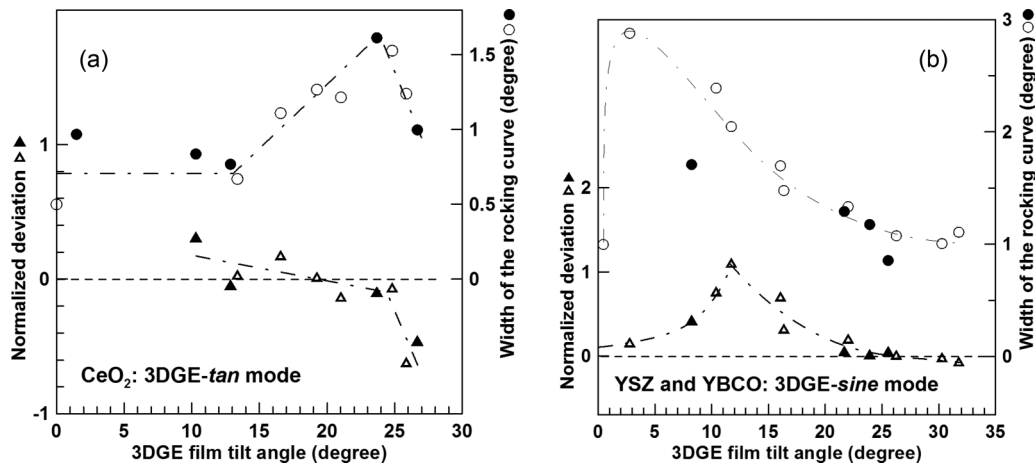


FIG. 13. Orientational properties of the 3DGE films with different growth mechanism. The overgrowth mechanism (a) shows an increase of the rocking curve width accompanied by a slow decrease of the deviation from positive to negative values until after the threshold angle FWHM of rocking curve decreases and the negative deviation rapidly increases. Open symbols: CeO<sub>2</sub> films on NGO TAS, solid symbols: CeO<sub>2</sub> films on 3DGE YSZ film on NGO TAS. The simultaneous seeding mechanism (b) shows a gradual decrease of width of the rocking curve from very high level obtained at very low tilt angles. The deviation shows a peak at  $\sim 12^\circ$ . Note that the YBCO films (solid symbols) were deposited over a YSZ layer (with a CeO<sub>2</sub> interlayer), so the observed agreement between YBCO and YSZ (open symbols) data may be explained as inheritance of the properties of the bottom layer. The lines are given as guides for the eye.

1059 over two or more steps and the geometrical model (1) becomes  
1060 invalid.

1061 The dependencies for the sine model are completely dif-  
1062 ferent [Fig. 13(b)]. Even a small tilt of the substrate SICPs  
1063 results in a very broad rocking curve of the film. A very high  
1064 spread of the width of the rocking curve of the YSZ films on  
1065 a standard-oriented substrate [Fig. 6(b)] implies realization of  
1066 the 3DGE-sine mechanism even at very low tilt angles that are  
1067 always present on the surface of a standard-oriented substrate  
1068 due to inhomogeneous polishing. The rocking curves become  
1069 more and more narrow with an increase of the substrate tilt  
1070 until the FWHM of the rocking curves saturates at  $\sim 20^\circ$   
1071 (film tilt angle  $\sim 25^\circ$ ). The deviation from the calculated value  
1072 at this angle changes from positive to negative, but remains  
1073 small—no turn-down to the standard epitaxial relations was  
1074 observed for the 3DGE-sine growth mode in the whole studied  
1075 range, until  $\sim 35^\circ$ . The highest deviation is observed at  $5^\circ$ –  
1076  $10^\circ$  [film tilt  $\sim 12^\circ$ , Fig. 13(b)]. This dependence is well  
1077 explained by the simultaneous seeding mechanism. At high  
1078 tilt angles the seeding knots on the substrate surface form  
1079 a dense network, providing good conditions for seeding of  
1080 the grains with the exact tilt angle, determined by condition  
1081 (2). Both deviation and misorientation of the grains is small.  
1082 A decrease of the substrate tilt angle increases the distances  
1083 between the seeding knots and, hence, increases the width  
1084 of the distribution of  $d_s$ . An immediate consequence is the  
1085 increased misorientation of the grains of the film and, hence,  
1086 the width of the rocking curve. This tendency remains the  
1087 same until very small angles, when the standard growth mode  
1088 becomes dominant. Another consequence of the increased  
1089 distance between the seeding knots is a shift of the distribution  
1090 of the orientation of the grains towards higher tilt angles.  
1091 The reason is a higher probability of seeding of a grain of  
1092 a certain orientation when the distance between the seeding  
1093 knots is smaller, i.e., with higher tilt angle. This effect is  
1094 less influential when all distances  $d_s$  become long and the

1095 probability of seeding becomes even. For the YSZ films this  
1096 happens for substrate tilt angles below  $7^\circ$  (film tilt angle  
1097  $\sim 12^\circ$ ).

1098 YBCO on CeO<sub>2</sub> seems to grow in the 3DGE-sine mode  
1099 also (Fig. 11), but we could not observe the same effects  
1100 as for YSZ. The probable reason is the inheritance of the  
1101 tangent mode properties of the CeO<sub>2</sub> layer. The YBCO films  
1102 on a CeO<sub>2</sub>/YSZ bilayer shows dependencies similar to that  
1103 of YSZ [solid symbols in Fig. 13(b)] but, again, it may be a  
1104 consequence of the sine growth mode of the YSZ layer below.  
1105 The parameters of the YBCO films on a CeO<sub>2</sub>/YSZ bilayer  
1106 after normalization lies along the same lines as that of YSZ  
1107 3DGE films [Fig. 13(b)].

1108 An excess of film tilt ( $0.5^\circ$ – $1^\circ$ ) over the calculated using  
1109 the geometrical model was observed for CeO<sub>2</sub> on Ni in  
1110 [17]. The angular range for this excessive tilt increased with  
1111 deposition temperature  $T_D$  from  $1^\circ$ – $11^\circ$  at  $785^\circ\text{C}$ , to  $1^\circ$ – $15^\circ$   
1112 at  $700^\circ\text{C}$ , and  $2^\circ$ – $15^\circ$  at  $600^\circ\text{C}$  (the upper angular limit  
1113 for the excessive tilt is observed only for the highest  $T_D$ ).  
1114 Assuming simultaneous seeding over a step, we get higher  
1115 probability of seeding on long distances  $d_s$  with increased  $T_D$ ,  
1116 and, hence, a shift of the excessive tilt range to smaller tilt  
1117 angles.

#### 1118 D. Effect of surface features

1119 The 3DGE growth mechanism essentially depends on the  
1120 morphology of the substrate. Rigorous preparation of the  
1121 substrate surface by chemical etching and annealing at high  
1122 temperature (surface reconstruction) results in a regular  
1123 sequence of uniform steps one-unit-cell high. Such a substrate  
1124 provides the most refined conditions for testing certain growth  
1125 effects and mechanisms.

1126 Unfortunately, our depositions were performed on the sub-  
1127 strates with no special treatment to form the SICP-faceted  
1128 growth steps. The substrate showed a very smooth surface,



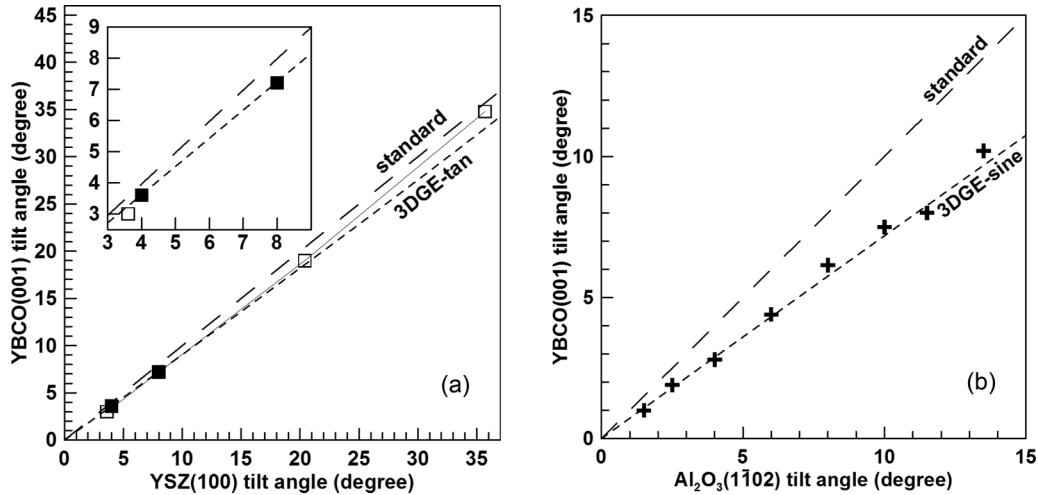


FIG. 14. Examples of 3DGE growth in studies of other groups. (a) YBCO deposition over YSZ TAS with (open squares, [23]) and without (solid squares, [22])  $Y_2O_3$  buffer layer. (b) YBCO deposition over  $CeO_2$  layer on sapphire TAS [22]. Note that  $Y_2O_3$  over YSZ and  $CeO_2$  over sapphire grow in the standard mode.

with roughness  $R_a$  less than  $2 \text{ \AA}$ , with no oriented or elongated features even for the TAS with high tilt angle. Observation of such a morphology implies the presence of damaged “amorphous” areas at least on some part of the substrate surface. Applicability of the geometrical growth mechanisms [Figs. 1(b) and 1(c)] was under serious doubts. Still the 3DGE growth mechanism was reliably detected for the majority of the tested top layer/bottom layer combinations. We may conclude, that even substrates that were not undergoing the surface reconstruction procedure provide good enough conditions for realization of the 3DGE growth. In fact, the 3DGE mechanism was *not* observed only when the bonds between film and bottom layer were broken by intense chemical interaction (YBCO on YSZ, and, for some deposition conditions, on  $CeO_2$  and BZO), and when the film and substrate were of the same crystal structure and the lattice mismatch between them was small  $\sim 1\%$  (YBCO on NGO).

Considering the effect of the surface morphology on the formation of the 3DGE films, we notice that even after severe step bunching ( $5^\circ$  tilted from (0001) plane sapphire substrates after annealing at  $1500^\circ C$  showed steps  $\sim 40 \text{ \AA}$  high [15]) the substrates provided good enough conditions for the 3DGE growth, i.e., both damaged amorphous surfaces and high steps after step bunching still allow growth by the 3DGE mode, implying a very high tolerance of this growth mode to the surface conditions.

One more important issue referring to the substrate surface preparation is the orientation of the tilt axis. In our experiments the tilt axis was quite close to the [001] axis of the substrate, providing good conditions for “initial” matching of the film and substrate lattices. We cannot confidently claim that the film orientation will follow the 3DGE growth mode if the tilt axis is chosen along some other crystallographic direction. It is known that the change of the orientation of the surface features can influence orientation of the growing films (see, e.g., [32–34]). Experiments in semiconductor heterostructures showed a broad variety of effects of changing the tilt axis direction in the habit plane. Already in [8] the 3DGE growth mode of Ga(In)As was observed along the  $(-110)$  direction

on the GaAs (001) plane, but not along orthogonal  $\{110\}$  direction. In [11]  $CdS_2$  growth on sapphire showed 3DGE growth for all orientations of the tilt axis, while Si on sapphire, similarly to [8], showed the 3DGE behavior for tilt along only one of two orthogonal directions. The reason was different surface morphology resulting from miscut in nonsymmetric crystallographic directions [11]. The most complicated film tilt mechanism was observed in [35], when misfit level changed not only the film tilt angle, but also direction of tilt as seen from the habit plane. Ni grains orientations in [17] were “randomly” distributed along a predominant orientation, so the tilt axes on different grains were randomly oriented in the habit plane. All  $CeO_2$  grains showed the same 3DGE growth mode, implying completely isotropic behavior of ceria on Ni [17]. In our case changing the tilt axis to [111] ( $45^\circ$  tilt from the [001] direction in the (110) habit plane of NGO) may result in 3DGE growth with the same relations along the habit plane, or  $45^\circ$  tilt of the film axes in habit plane, or in  $45^\circ$  tilt of the film axes normal to the habit plane—all these initial orientational relations are possible and should be checked experimentally for each pair top layer/bottom layer. We even cannot claim that the 3DGE mechanism would be preserved if the tilt axis is changed.

### E. Evidences of 3DGE growth in all-metaloxide heterostructures in the literature

In the Introduction part of this paper we mentioned some observations of the 3DGE growth mode by other groups. In fact, these observations are more numerous, but sometimes these data were misinterpreted or left without explanation.

In [22] two combinations film-substrate (YBCO/YSZ and YBCO/ $CeO_2$ /Al<sub>2</sub>O<sub>3</sub>) were studied in a wide angular range,  $0^\circ$ – $14^\circ$ , orientation of both is finely described by the 3DGE growth mechanism. YBCO grows over YSZ in the same way as YBCO over  $CeO_2$  in our experiments, with formation of Ba(Zr, Y)O<sub>3</sub> interlayer aligned with the YSZ SICPs [Fig. 14(a), solid squares]. YBCO over  $CeO_2$  follows the 3DGE-sine growth mode assuming no chemical

1205 interaction between YBCO and CeO<sub>2</sub>, but CeO<sub>2</sub> grows on  
 1206 sapphire according to the standard mode, with parallel SICPs :  
 1207 (001) CeO<sub>2</sub> || (1 - 1 0 2) Al<sub>2</sub>O<sub>3</sub> [Fig. 14(b)]. Actually, agree-  
 1208 ment with the 3DGE-tangent mode is marginally better, but  
 1209 we decided to keep the sine model in agreement with our  
 1210 results. Anyway, the difference between the sine and tangent  
 1211 modes in the 0°–14° range is less than 0.15°, being hardly  
 1212 distinguishable without special precautions during measure-  
 1213 ment. Note that a very good agreement is obtained using  
 1214 lattice constants for YBCO (11.685 Å), YSZ (5.149 Å), CeO<sub>2</sub>  
 1215 (5.405 Å), and Ba(Y, Zr)O<sub>3</sub> (4.31 Å), as measured in our  
 1216 experiments. No attempts to improve conformity by fitting the  
 1217 lattice constants was done.

1218 Another example of 3DGE growth is presented in [23].  
 1219 The YBCO films buffered by a Y<sub>2</sub>O<sub>3</sub> layer on a YSZ TAS  
 1220 showed a pronounced tilt of the SICP from the habit plane  
 1221 of the substrate in the range 3°–36°. Again we get a good  
 1222 agreement between the presented numbers and calculated using  
 1223 formula (1), assuming chemical interaction with formation  
 1224 of Ba(Y, Zr)O<sub>3</sub> with the same orientation of the SICP as that  
 1225 of the substrate and buffer layer [Fig. 14(a), open squares].  
 1226 A tendency towards standard growth mode is observed at  
 1227 high angles, similarly to our results with BZO deposition on  
 1228 NGO TAS (Fig. 7), so we used the tangent model for the  
 1229 calculation. The agreement with the geometrical model is less  
 1230 accurate compared to [22] results, either due to an unknown  
 1231 composition of the product of chemical interaction in the  
 1232 beginning of the YBCO film growth, or simply as a result of  
 1233 the approximate numbers given in [23].

1234 Deposition of YBCO on YSZ layer in our experiments al-  
 1235 ways resulted in *c*-oriented YBCO films, in contradiction with  
 1236 the results [22], where 3DGE growth started after initial chem-  
 1237 ical interaction with formation of Ba(Y, Zr)O<sub>3</sub> layer. Yttrium  
 1238 segregation on the YSZ substrate surface during substrate  
 1239 preparation may be the reason, forming a Y(Zr)<sub>2</sub>O<sub>3</sub>/YSZ  
 1240 surface layer similar to Y<sub>2</sub>O<sub>3</sub>/YSZ in [23]. Such segregation  
 1241 is expected at high oxygen partial pressure, during annealing  
 1242 of the substrates after CMP, or during the prebake step im-  
 1243 mediately before deposition [36].

1244 Theis and Schlom [24] present a much more complicated  
 1245 heterostructure, where tetragonal PbTiO<sub>3</sub> grows on a SrTiO<sub>3</sub>  
 1246 TAS in two different orientations. Accurate modeling of the  
 1247 growth mode demands precise measurement of the lattice  
 1248 constants that are affected by stoichiometry and substrate-  
 1249 induced strain. Still the agreement with the geometrical model  
 1250 is more than qualitative. In [37] a significant distortion of the  
 1251 lattice should be taken into account to obtain agreement be-  
 1252 tween the geometrical model and the observed data. Reference  
 1253 [35] also notes importance of possible tetragonal distortions  
 1254 introduced by the substrate. These experiments demonstrate  
 1255 that the good agreement between calculated and measured  
 1256 values in our experiments is, in some sense, a coincidence,  
 1257 at least when such materials as CeO<sub>2</sub> are considered. The  
 1258 structure of CeO<sub>2</sub> is easily distorted by the substrate-induced  
 1259 strain, and the lattice constant of ceria strongly depends on  
 1260 density of oxygen vacancies generated during deposition (see,  
 1261 e.g., [17,31,38]). Reasonable agreement of the experimental  
 1262 data with the simplified model (1) is, to some extent, a for-  
 1263 tunate combination of circumstances, including oxygenation  
 1264 during and after deposition, and thickness of the films high

1265 enough to ignore the substrate-induced strain in the interface  
 1266 area.

1267 The possible effect of lattice distortion can be illustrated  
 1268 with results of [18] [see Fig. 2(a)]. The critical angle  $\gamma_c$ ,  
 1269 calculated using standard ceria lattice constant, is smaller than  
 1270 the observed one (30.4° and 32°, respectively). Taking into ac-  
 1271 count tetragonal distortion of ceria by the substrate-introduced  
 1272 tensile strain [assuming volume-preserving distortion and  
 1273 strain introduction only along the habit plane (110) NGO],  
 1274 we obtain  $\gamma_c = 31.2^\circ$ , in better agreement with the measured  
 1275 value. In fact, such estimation should consider also the strain  
 1276 introduced by the edges of the steps on the substrate surface,  
 1277 a decrease of the unit cell volume in the strained lattice, and  
 1278 expansion of the lattice due to oxygen nonstoichiometry dur-  
 1279 ing deposition. All these factors are decreasing the calculated  
 1280  $\gamma_c$ , so the accurate estimation would be in between 30.4°  
 1281 and 31.2°. For our CeO<sub>2</sub> films fabricated by PLD we do not  
 1282 observe a substantial tetragonal distortion. The ceria lattice  
 1283 constant measured along the normal to habit plane (110)  
 1284 NGO showed no dependence on angle and remained close to  
 1285 the value measured for the standard-oriented substrate. With  
 1286 increasing tilt angle the effect of mismatch with the habit  
 1287 plane is decreasing, and the counteracting strain introduced by  
 1288 the step edges is increasing. Constant lattice parameter, thus,  
 1289 means that the film grows independently on the substrate-  
 1290 induced strain and the lattice constant depends mainly on the  
 1291 deposition conditions (and corresponding density of oxygen  
 1292 vacancies in the film). An indirect proof of weak effect of  
 1293 tetragonal distortion for our films is a good match between  
 1294 the calculated and measured film tilt values (Fig. 4).

1295 Hoek *et al.* [39] provide another example of a more compli-  
 1296 cated mechanism matching top and bottom layers. The SICPs  
 1297 of La(Sr)CuO<sub>4</sub> grown on a 26° ramp etched of Nd(Ce)CuO<sub>4</sub>  
 1298 demonstrated a 3.3° inclination to the SICPs of the bottom  
 1299 layer. The inclination monotonously changes with the tilt  
 1300 angle of the ramp. The geometry of growth and the behavior  
 1301 of the inclination are similar to that discussed in our study, but  
 1302 application of the simple geometrical model gives a smaller  
 1303 tilt angle of 2.8°. Authors [39] suggest a more sophisticated  
 1304 mechanism of matching of corresponding facets, say, (3 0 19),  
 1305 of the top and bottom layers during growth, with simultaneous  
 1306 matching of both in-plane and out-of-plane lattice constants.  
 1307 This approach provides excellent agreement with the observed  
 1308 tilt angle between the SICPs of two layers. Similar results can  
 1309 be obtained for twin boundaries [39], where facet matching is  
 1310 the obvious mechanism of strain accommodation on the grain  
 1311 boundaries. References [11] and [40] also point out matching  
 1312 at higher symmetries (symmetric [11] and asymmetric [40]  
 1313 boundaries) as an alternative to the simple geometrical match-  
 1314 ing at the film-substrate interface.

## 1315 V. CONCLUSION

1316 We studied growth by PLD of metaloxide thin films on  
 1317 NdGaO<sub>3</sub> substrates with the surface tilted from the stan-  
 1318 dard (110) crystallographic plane. Eight of ten studied top  
 1319 layer/bottom layer combinations showed a growth mode re-  
 1320 sulting in an inclination between the SICPs of the top layer  
 1321 and the corresponding SICPs of the bottom layer. The ob-  
 1322 served dependence of top layer tilt angle on the tilt angle of  
 1323

1323 the bottom layer is well explained by a simple geometrical  
1324 growth model, taking into account faceting of the surface  
1325 of the bottom layer. The resulting growth mode depends  
1326 both on standard atom-on-atom epitaxial matching along the  
1327 tilt axis, graphoepitaxial matching in the normal to tilt axis  
1328 direction in the substrate plane, and on the ratio of growth  
1329 steps heights of the top and bottom layer, i.e., the matching  
1330 of the top and the bottom layer is three dimensional. This  
1331 growth mechanism may be described as a three-dimensional  
1332 graphoepitaxial (3DGE) growth.

1333 The 3DGE growth mechanism seems to be quite common  
1334 for deposition on TAS with tilt angles more than  $5^\circ$ . PLD,  
1335 rf sputtering [19,20], e-beam evaporation [18], and even LPE  
1336 [15] provided conditions good enough for the 3DGE growth.  
1337 No special substrate treatment is needed, even substrates with  
1338 damaged amorphous surface or with step bunching [15] are  
1339 suitable. The 3DGE growth mechanism is observed in mul-  
1340 tilayer structures, both when the bottom layer follows 3DGE  
1341 mode and when it grows with standard epitaxial relations. The  
1342 3DGE growth was observed both with increase and decrease  
1343 of the top layer tilt angle compared to the tilt angle of the  
1344 bottom layer.

1345 Two different 3DGE dependencies may be distinguished  
1346 in the high-angle range ( $>15^\circ$ ): with a tendency towards  
1347 standard growth above some threshold angle, and retaining  
1348 3DGE behavior until a tilt angle of  $45^\circ$  is reached, either  
1349 by top or by bottom layer. The first type is better described  
1350 by a tangent angular dependence, and usually is observed

1351 when a compressive strain is induced in the top layer. The  
1352 second type follows a sine dependence, and is usually seen  
1353 for tensile-strained top layers. An increase over the calcu-  
1354 lated value tilt is often observed in the range  $5^\circ$ – $10^\circ$  for the  
1355 sine-type dependencies. In a simplified way the difference  
1356 may be attributed to two different formation mechanisms,  
1357 “overgrowth” and “simultaneous seeding.” The first one forms  
1358 the tilt different from the bottom layer when the growing  
1359 grain overgrows another grain. For the second mechanism  
1360 the top layer tilt is formed right when the grain is seeded.  
1361 Some material combinations showed both dependencies, for  
1362 different deposition conditions. The reasons for realization of  
1363 each of these dependencies should be clarified.

1364 The results presented in this paper were obtained for ma-  
1365 terials with a simple cubic lattice (or the lattice that can be  
1366 reduced to a pseudocubic during growth at high deposition  
1367 temperature). Reports from other groups point to the fact  
1368 that a simple geometrical model of 3DGE growth may be of  
1369 limited validity in cases of more complex lattices, when the  
1370 top layer experiences significant distortions due to a bottom  
1371 layer induced strain, or when the boundary between two layers  
1372 exhibits mirror or central symmetry.

#### ACKNOWLEDGMENTS

1373  
1374 The work was supported by Program of FASO of Russia.  
1375 I.K.B. also wishes to acknowledge FCT for its financial  
1376 support (Grant No. IF/00582/2015).

- 
- [1] C. Tegenkamp, *J. Phys.: Condens. Matter* **21**, 013002 (2009).  
 [2] M. Mukaida, Sh. Miyazawa, and M. Sasaura, *Jpn. J. Appl. Phys.* **30**, L1474 (1991).  
 [3] J. Brotz, H. Fuess, T. Haage, J. Zegenhagen, Ch. Jooss, A. Forkl, and R. Warthmann, *J. Appl. Phys.* **85**, 635 (1999).  
 [4] H. Song and T. S. Sudarshan, *J. Cryst. Growth* **371**, 94 (2013).  
 [5] J. Zegenhagen, T. Haage, and Q. D. Jiang, *Appl. Phys. A* **67**, 711 (1998).  
 [6] Ch. Chen, Zh. Chen, J. Zhang, and X.-J. Du, *Sci. China Phys. Mech. Astron.* **55**, 2042 (2012).  
 [7] O. Igarashi, *J. Appl. Phys.* **42**, 4035 (1971).  
 [8] H. Nagai, *J. Appl. Phys.* **45**, 3789 (1974).  
 [9] G. H. Olsen and R. T. Smith, *Phys. Status Solidi A* **31**, 739 (1975).  
 [10] O. Igarashi, *Jpn. J. Appl. Phys.* **15**, 1435 (1976).  
 [11] M. Aindow and R. C. Pond, *Philos. Mag. A* **63**, 667 (1991).  
 [12] F. Riesz, *J. Appl. Phys.* **79**, 4111 (1996).  
 [13] J. P. Hirth and R. C. Pond, *Philos. Mag.* **90**, 3129 (2010).  
 [14] A. Petkova, J. Wollschlaeger, H.-L. Guenter, and M. Henzler, *Surf. Sci.* **542**, 211 (2003).  
 [15] R. Bachelet, G. Nahelou, A. Boule, R. Guinebretiere, and A. Dager, *Prog. Solid State Chem.* **33**, 327 (2005).  
 [16] I. K. Bdikin, J. E. Mozhaeva, P. B. Mozhaev, C. S. Jacobsen, J. Bindslev Hansen, A. L. Kholkin, V. A. Luzanov, and I. M. Kotelyanskii, report on MATERIALS 2005: XII Portuguese Materials Society Meeting, III International Materials Symposium, Aveiro, Portugal, 2005 (unpublished).  
 [17] J. D. Budai, W. Yang, N. Tamura, J.-S. Chung, J. Z. Tischler, B. C. Larson, G. E. Ice, Ch. Park, and D. P. Norton, *Nat. Mater.* **2**, 487 (2003).  
 [18] I. M. Kotelyanskii and V. A. Luzanov (private communication, 1996).  
 [19] I. K. Bdikin, P. B. Mozhaev, G. A. Ovsyannikov, F. V. Komissinskii, I. M. Kotelyanskii, and E. I. Raksha, *Phys. Solid State* **43**, 1611 (2001).  
 [20] I. K. Bdikin, P. B. Mozhaev, G. A. Ovsyannikov, P. V. Komissinskii, and I. M. Kotelyanskii, *Physica C* **377**, 26 (2002).  
 [21] P. B. Mozhaev, J. E. Mozhaeva, I. K. Bdikin, I. M. Kotelyanskii, V. A. Luzanov, J. Bindslev Hansen, C. S. Jacobsen, and A. L. Kholkin, *Physica C* **434**, 105 (2006).  
 [22] E. Stepantsov, M. Tarasov, A. Kalabukhov, L. Kuzmin, and T. Claeson, *J. Appl. Phys.* **96**, 3357 (2004).  
 [23] C. H. Mueller, P. H. Holloway, J. D. Budai, F. A. Miranda, and K. B. Bhasin, *J. Mater. Res.* **10**, 810 (1995).  
 [24] C. D. Theis and D. G. Schlom, *J. Mater. Res.* **12**, 1297 (1997).  
 [25] S. Kim, Y. Kang, and S. Baik, *Thin Solid Films* **256**, 240 (1995).  
 [26] P. B. Mozhaev, A. V. Khoryushin, J. E. Mozhaeva, J.-C. Grivel, J. Bindslev Hansen, and C. S. Jacobsen, *J. Supercond. Novel Magnetism* **30**, 2401 (2017).  
 [27] P. B. Mozhaev, J. E. Mozhaeva, I. K. Bdikin, T. Donchev, E. Mateev, T. Nurgaliev, C. S. Jacobsen, J. Bindslev Hansen, S. A. Zhgoon, and A. E. Barinov, *Proc. SPIE* **5401**, Micro- and Nanoelectronics 2003 (2004).  
 [28] J. A. Alarco, G. Brorsson, Z. G. Ivanov, P.-A. Nilsson, E. Olsson, and M. Lofgren, *Appl. Phys. Lett.* **61**, 723 (1992).

- [29] J.-H. Kim, S. Oh, and D. Youm, *Thin Solid Films* **305**, 304 (1997).
- [30] E. I. Givargizov, *Thin Solid Films* **189**, 389 (1990).
- [31] F. Wu, A. Pavlovska, D. J. Smith, R. J. Culbertson, B. J. Wilkens, and E. Bauer, *Thin Solid Films* **516**, 4908 (2008).
- [32] G. Brorsson, E. Olsson, Z. G. Ivanov, E. A. Stepantsov, J. A. Alarco, Yu. Boikov, T. Claeson, P. Berastegui, V. Langer, and M. Loefgren, *J. Appl. Phys.* **75**, 7958 (1994).
- [33] D. Vassiloyannis and P. M. Pardalos, *Physica C* **468**, 147 (2008).
- [34] M. Sunder and P. D. Moran, *J. Electron. Mater.* **38**, 1931 (2009).
- [35] A. Pesek, K. Hinger, F. Riesz, and K. Lischka, *Semicond. Sci. Technol.* **6**, 705 (1991).
- [36] X.-G. Wang, *Surf. Sci.* **602**, L5 (2008).
- [37] D. A. Neumann, H. Zabel, and H. Morkoc, *J. Appl. Phys.* **64**, 3024 (1988).
- [38] D. P. Norton, C. Park, J. D. Budai, S. J. Pennycook, and C. Prouteau, *Appl. Phys. Lett.* **74**, 2134 (1999).
- [39] M. Hoek, F. Coneri, N. Poccia, X. Renshaw Wang, X. Ke, G. Van Tendeloo, and H. Hilgenkamp, *Appl. Phys. Lett. Mater.* **3**, 086101 (2015).
- [40] B. W. Dodson, D. R. Myers, A. K. Datye, V. S. Kaushik, D. L. Kendall, and B. Martinez-Tovar, *Phys. Rev. Lett.* **61**, 2681 (1988).